Mathematical Biosciences and Engineering

https://www.aimspress.com/journal/mbe

MBE, 23(6): 1651–1686.
DOI: 10.3934/mbe.2026060
Received: 03 June 2025
Revised: 08 January 2026
Accepted: 15 February 2026
Published: 06 May 2026

Research article

A simple mechanistic model for insulin-glucose-glucagon dynamics and its implications for diabetes management

Mackenzie Dalton, Emmanuel Asante-Asamani and James Greene*

Department of Mathematics, Clarkson University, NY 13699, USA

* **Correspondence:** Email: jgreene@clarkson.edu.

Abstract: Insulin and glucose dynamics are tightly regulated by the pancreatic islets of Langerhans, which contain beta cells that produce insulin and alpha cells that produce glucagon. Insulin lowers blood glucose by enabling cells to access glucose for energy, while glucagon raises blood glucose levels by stimulating the liver to produce glucose from non-carbohydrate sources as well as breaking down stored glycogen. Maintaining safe blood glucose levels is crucial, as both high (hyperglycemia) and low (hypoglycemia) levels can lead to life threatening consequences. In this work, a simple three-state mechanistic insulin-glucose-glucagon model is developed and validated using data from pigs subjected to an intravenous glucose tolerance test (IVGTT). The model is then used to investigate glucose and glucagon dynamics in patients administering exogenous insulin, shedding light on the impact of improper diabetes management. The results show that delayed administration of exogenous insulin increases the risk of hypoglycemia by suppressing glucagon production. Furthermore, insulin half-lives of 60 minutes or longer were tested, revealing that such prolonged exogenous insulin activity can suppress glucagon's response to critically low glucose levels. This finding suggests that shorter insulin half-lives may help reduce the risk of hypoglycemic events.

Keywords: glucagon; insulin; glucose; differential equations; diabetes; mathematical modeling

1. Introduction

Blood glucose levels are a crucial component of homeostatic regulation. Therefore, maintaining normal blood glucose levels is critical to health. The regulation of glucose levels in the body is accomplished through a complex interplay of hormones, primarily insulin and glucagon, secreted by the pancreas. These hormones work together to ensure that blood glucose levels remain within a narrow and well-defined range. The significance of maintaining healthy glucose levels cannot be overstated, as levels outside a healthy range can have severe consequences. Abnormally high blood glucose levels, known as hyperglycemia, can lead to a range of complications such as cardiovascular

diseases, kidney dysfunction, and nerve damage [1, 2]. In extreme cases, uncontrolled hyperglycemia can lead to diabetic ketoacidosis (DKA) which is life-threatening and is the leading cause of death in children with type 1 diabetes [3]. On the other hand, hypoglycemia, characterized as an abnormally low blood glucose level, can be deadly. Glucose is the primary energy source for the brain and other vital organs. When blood glucose levels decrease significantly, symptoms such as dizziness, confusion, and, in severe cases, loss of consciousness may result. In situations where the body cannot access an adequate supply of glucose, the consequences may be fatal [4].

The pancreatic islets of Langerhans are cell clusters found in the pancreas that respond to glucose levels by secreting either a blood glucose lowering hormone, insulin, or a blood glucose raising hormone, glucagon [5]. Alpha (α) cells, beta (β) cells, and delta (δ) cells are the primary cells composing the pancreatic islets of Langerhans, each of which respond to both increases and decreases in blood sugar levels [5]. To raise blood glucose levels, the pancreatic α cells secrete the hormone glucagon, also known as anti-insulin. Glucagon works by triggering the liver to convert stored glucose (glycogen) into glucose, which is then released into the bloodstream; this process is known as glycogenolysis [6]. Moreover, glucagon can also raise blood glucose levels by preventing the liver from absorbing and storing glucose so that more glucose remains in the blood stream [6]. To lower blood glucose levels, the pancreatic β cells secrete the hormone insulin. Insulin works by acting as a "key" that allows glucose to enter into a cell and subsequently lowers blood glucose levels. Without insulin, glucose cannot enter the cell [7]. Moreover, insulin blocks the production of glucagon from α cells , which leads to a reduced production of glucose by the body [8].

Diabetes is a disease where the body either becomes resistant to insulin (type 2) or there is a low/absent production of insulin due to an autoimmune attack on the insulin producing β cells (type 1). In the latter case, and occasionally in the former as well, the patient requires insulin injections in order to regulate blood glucose levels which therefore results in the loss of the direct feedback of glucose on insulin production. This loss of communication results in a disregulation of glucagon dynamics, despite α cells remaining functional [9]. In fact, on average, patients with type 1 diabetes administering exogenous insulin experience two symptomatic hypoglycemic events a week and about one severe event a year which requires assistance from another person [10]. Hence, for those on insulin therapy, hypoglycemia remains a major roadblock to euglycemic control. The lack of response to hypoglycemic events in patients administering exogenous insulin is still poorly understood [10].

In 1979 Richard Bergman and colleagues introduced minimal models of insulin dynamics and of glucose kinetics [11] to understand their response to an intravenous glucose tolerance test (IVGTT). The test involves an injection of glucose into the bloodstream followed by the monitoring of blood glucose and insulin levels for a period of time, and can aid in the diagnosis of type 2 diabetes by calculating an individual's insulin sensitivity—a measurement of the ability of insulin to stimulate the uptake of glucose. In this work, we refer to the combination of the minimal insulin model and minimal glucose model as the minimal model. While this model is still utilized as of writing, it does possess limitations. Two of the main criticisms of the minimal model are that (a) insulin production is explicitly time-dependent, and hence the model is only applicable during the IVGTT, and (b) a non-observable remote insulin compartment is introduced that aims to model the insulin-dependent uptake of glucose [12]. Beyond the minimal model, there have been a variety of other models that aim to describe insulin-glucose dynamics [12–15]; we note that the authors of [15] take a similar

approach to the work presented here, in that they construct a three-compartment mathematical model to understand the homeostasis of glucose and insulin, and utilize data from healthy rats to estimate physiological parameters.

In alignment with the growing biological research on glucagon, additional models have been introduced to explore the relationship between insulin, glucose, and glucagon. However, many of these models either directly extend the minimal model [16–19] or eliminate the remote insulin compartment [12–14, 20], a fundamental feature of the minimal model. In [12, 21], new models of insulin and glucose are introduced which do not incorporate the effects of glucagon. Furthermore, models incorporating glucagon have been proposed, but many of these models still present certain limitations. For example, in [13, 20, 22, 23] the authors consider additional biological details such as diet and exercise, which are not relevant during the IVGTT. Glucagon and c-peptide dynamics were modeled in [24], the latter of which serves as a proxy for endogenous insulin secretion. In this work, our objective is to understand the impact of external insulin, and thus we directly model insulin, and not c-peptide. As another alternative to the minimal model, a number of works, largely inspired by De Gaetano and colleagues, introduce explicit time delays in insulin secretion due to elevated glucose levels [21, 25–28]; see [14] for a recent review of mathematical models of glucose dynamics for systems of delay differential equations. Time delays are indeed intrinsic to the regulation of hormones, and long-term oscillatory behavior may not be able to be understood without incorporating them into mathematical models [29, 30]. However, we note that frameworks which include memory necessarily add complexity to both analysis and data fitting, when compared with their "memoryless" ordinary differential equations (ODEs) counterparts [31].

In this paper, we introduce an alternative modeling framework for insulin-glucose dynamics, which explicitly incorporates glucagon as a mechanistic regulator. In healthy individuals, insulin, glucose, and glucagon utilize feedback loops to maintain blood glucose levels, and our system of equations reflects the current understanding of the interactions of these three compounds. By incorporating in vivo data from 10 pigs subjected to the IVGTT, we validate our model and then use it to shed light on the dynamics of glucose and glucagon when administering exogenous insulin. As type 1 diabetes represents a specific disruption of the feedback of glucose on insulin, our model is ideally suited to study the nature of this disease with respect to exogenous insulin on time scales relevant for dose design.

2. Models

Here we present models for understanding the regulation of insulin, glucose, and glucagon, both in a healthy state (Section 2.1), and in a state where insulin is disregulated (Section 2.2).

2.1. A model for insulin-glucose-glucagon regulation

We develop a three-state model of insulin and glucose dynamics that includes insulin (I), glucose (G), and glucagon (G_ℓ). A schematic of the primary interactions we consider are provided in Figure 1. Here, glucose stimulates the production of insulin and insulin has a natural decay rate. High levels of both insulin and glucose suppress glucagon production, and glucagon also has a natural decay rate. Lastly, glucagon stimulates the production of glucose and glucose is cleared through both insulin-dependent and insulin-independent pathways.

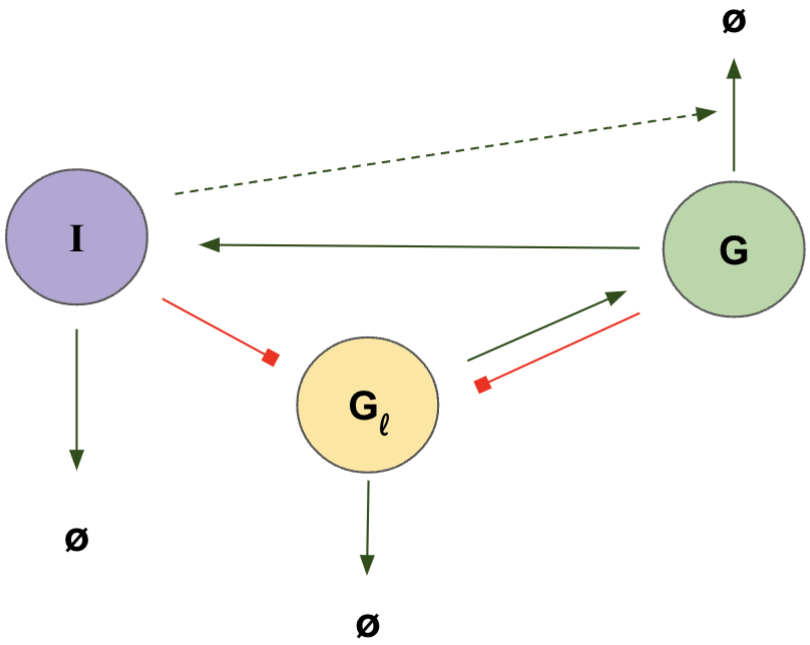

Figure 1. Schematic representing the interactions in the IGG models (2.1)–(2.3). G denotes the glucose concentration, I the insulin concentration, and G_ℓ the glucagon concentration.

We modeled these interactions with a system of three ODEs for insulin (I), glucose (G), and glucagon (G_ℓ) as follows:

$$\frac{dI}{dt} = \frac{k_1 G^n}{k_2^n + G^n} - \delta_1 I \tag{2.1}$$

$$\frac{dG}{dt} = k_3 G_\ell - (\delta_2 I + \delta_3) G \tag{2.2}$$

$$\frac{dG_\ell}{dt} = \frac{k_4}{1 + z(G - h)^+ + pI} - \delta_4 G_\ell \tag{2.3}$$

We refer to this model as the IGG model. Mass action kinetics are assumed for most interactions, unless otherwise specified. The major biological features of the model are the following:

1) Glucose stimulates the production of insulin [32]. The production of insulin was assumed to saturate as a function of glucose [33]. That is, the maximum insulin production rate (k_1) is independent of glucose. The exponent n represents the Hill coefficient which determines the steepness of insulin production as a function of glucose; larger n values correspond to a more binary response.

2) Insulin regulates the insulin dependent uptake of glucose ($\delta_2 I$) which is the primary mechanism by which glucose enters cells [34].

3) A small amount of glucose can enter cells through an insulin-independent uptake of glucose (δ_3) [34].

4) The production of glucagon is inhibited by both high levels of insulin and glucose [35]. This inhibition is modeled as the sum of two terms: pI, representing inhibition by insulin, and $z(G-h)^+$, representing inhibition by glucose. Here, p and z are non-negative constants. The glucose inhibition term $z(G-h)^+$ function is only active when $G > h$ to reflect the assumption that glucose only inhibits glucagon when it rises above a baseline level h. We note that experimental evidence suggests that glucagon secretion by α cells is suppressed nonlinearly [36, 37], but for simplicity, we assume first-order inhibitory feedback in the models (2.1)–(2.3). Recall that for any $x \in \mathbb{R}$, the positive part x^+ is defined as:

$$x^+ := \begin{cases} x, & x \geq 0 \\ 0, & x < 0 \end{cases}$$

5) The production of glucose in the body (that is, not due to a glucose injection) is regulated by glucagon ($k_3 G_\ell$) [38]. This occurs via glucagon signaling to the liver to break down stored glucose and releasing it into the bloodstream [6].

6) Insulin and glucagon both decay naturally (δ_1 and δ_4, respectively) [39, 40].

We note that we have also developed a two-state model of insulin and glucose to assess the necessity of glucagon in explaining insulin-glucose dynamics; see Section A.3. Results suggest that three states are needed to fully capture the utilized experimental data (see Figure A2), and hence in the remainder of the paper, we consider the three-state IGG models (2.1)–(2.3), as well as models derived from the IGG model (see Section 2.2).

Table 1 below provides both a description and the units for the species of the IGG model. For information on specific parameters (including estimated values), see Table 2, which is discussed in detail in Section 3.2.

Table 1. Description and units for species in the IGG models (2.1)–(2.3).

Species	Description	Units
G	Glucose concentration	$\frac{mmol}{L}$
I	Insulin concentration	$\frac{\mu g}{L}$
G_ℓ	Glucagon concentration	$\frac{pmol}{L}$

2.2. A modified IGG model describing disease

Patients with insulin-dependent diabetes administer exogenous insulin, which removes glucose's direct feedback on insulin. Thus we modify our model to mimic this scenario, where insulin is now treated as an external input into the system; see Figure 2 for a schematic. We are thus analyzing a system where the communication between insulin and glucose is disrupted, so that insulin can be considered an external input, which operates independently of glucose (G) and glucagon (G_ℓ). For

clarity, we denote this external insulin concentration with the symbol $\hat{I} = \hat{I}(t)$. This reduced model takes the form of a two-dimensional system with external input $\hat{I}$:

$$\frac{dG}{dt} = k_3 G_\ell - (\delta_2 \hat{I}(t) + \delta_3) G \tag{2.4}$$

$$\frac{dG_\ell}{dt} = \frac{k_4}{1 + z(G-h)^+ + p\hat{I}(t)} - \delta_4 G_\ell \tag{2.5}$$

We refer to this model as the diseased insulin-glucose-glucagon model (dIGG). Note here that Eqs (2.4)–(2.5) are precisely the equations for glucose and glucagon in our proposed IGG models (2.2)–(2.3), with the only difference being that insulin is now considered as external input; our goal is to thus study the system during disease, which corresponds to removing the feedback between glucose and insulin.

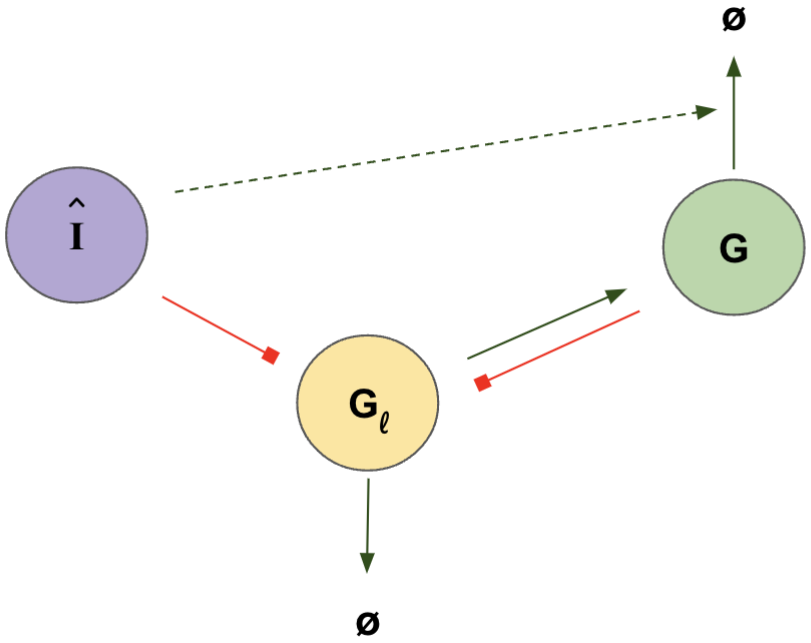

Figure 2. Schematic of the dIGG models (2.4)–(2.5). Here, insulin is considered as an external input to the system ($\hat{I}$), so that glucose no longer regulates insulin production (compare to Figure 1)

3. Methods

3.1. Experimental data

We utilized data collected from a study conducted by Manell et al. [41], where ten pigs were subjected to an intravenous glucose tolerance tests (IVGTT). These pigs underwent measurements of insulin, glucose, and glucagon, which were taken both before glucose infusion and at 2, 5, 10, 20, 30,

45, 60, 90, 120, and 180 minutes post infusion. Of the ten pigs, the final glucagon measurement was missing for three of them. At each time point, we calculated the median across the 10 pigs for insulin, glucose, and glucagon; the median was utilized to account for the large variability of the glucagon measurements. Denoting the time points via t_i, $i = 1, 2, \ldots, N$, the experimental data consists of tuples of the form $(t_i, I^{d,i}, G^{d,i}, G_\ell^{d,i})_{i=1}^N$. For example, $G^{d,i}$ denotes the median glucose level at time t_i. Furthermore, we computed a 95% confidence interval with respect to the median via bootstrapping [42]. Specifically, we generated 10,000 new data sets, with each set consisting of 10 pigs. We then calculated the median of each new data set to generate 10,000 medians which yielded a distribution of the medians at each time point. From this data we constructed a sampling distribution for the median, which was used to calculate the 95% confidence interval. The pig data, together with the median and estimated confidence intervals, are provided in Figure 3. We highlight that while glucose and insulin exhibited minimal variation over time, the levels of glucagon displayed substantial variability, particularly during the 30 minutes following the IVGTT.

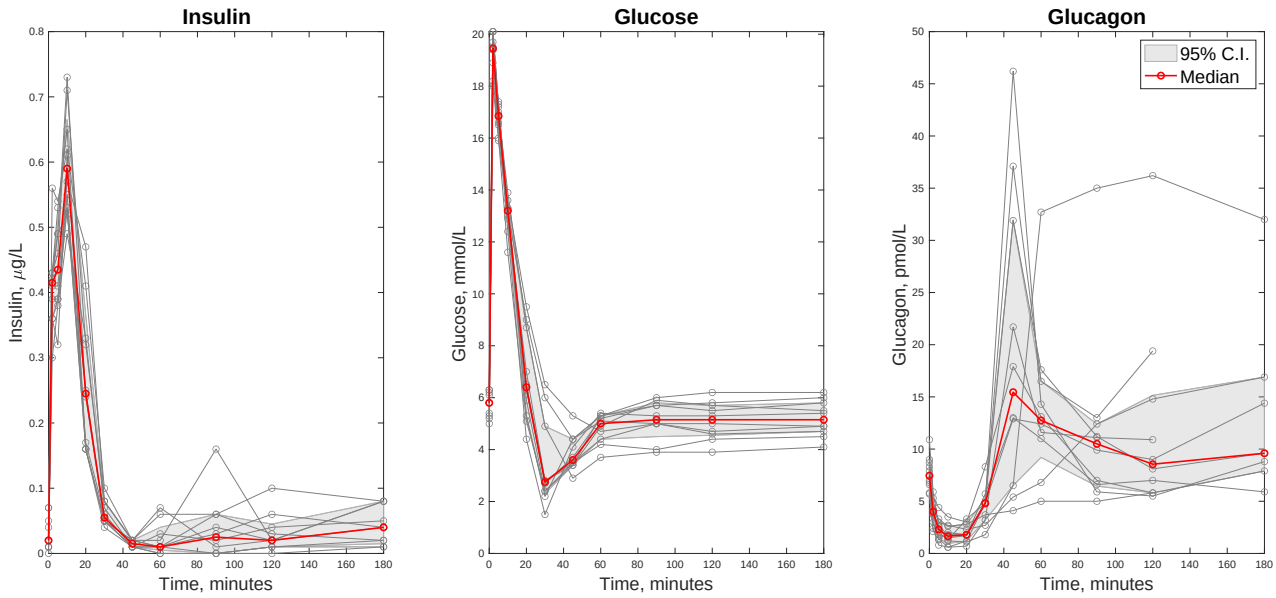

Figure 3. Experimental data. Plot of the pig data (insulin, glucose, and glucagon over a 180 minute period), medians, and estimated 95% confidence intervals for an IVGTT. Left plot shows insulin, middle shows glucose, and right shows glucagon.

3.2. Parameter estimation

To estimate rate parameters in the IGG model, we fit to the median of the pig data presented in Section 3.1. We used the median to avoid outliers skewing the estimated parameter values, particularly with respect to glucagon, where the measurements exhibited a large variance (see Figure 3). To simulate a glucose injection from the IVGTT, we incorporate an external input $u(t)$

(units of mmol/L/min) into the glucose component of the IGG model (Eq (2.2)) of the form

$$u(t) = \begin{cases} \bar{u}, & t \in [t_0, t_0 + T] \\ 0, & \text{otherwise} \end{cases}. \tag{3.1}$$

Here, $\bar{u}$ is the applied (constant) dosage rate which was taken to match the peak glucose value of the experimental data, t_0 is start time of the dosage, and T is the length of the infusion. In this case, we replace Eq (2.2) with

$$\frac{dG}{dt} = k_3 G_\ell - (\delta_2 I + \delta_3)G + u(t). \tag{3.2}$$

Note that we are not modeling the pharmacokinetics of glucose; hence u represents an "effective" dose rate. As discussed in [41], the length of the applied glucose injection was 1 minute, beginning at minute 0 of the experiment. Referring to (3.1), we thus set $t_0 = 0$ and $T = 1$ minute. To translate between the applied and effective doses, we computed the difference between glucose levels at times 0 and 2 minutes and added a constant of $c = 1$ mmol/L to this difference so as to account for glucose loss during infusion; $\bar{u}$ was then defined as this glucose level scaled by the infusion duration T. Referring to the notation for the experimental data as discussed in Section 3.1, we thus set

$$\bar{u} := \frac{G^{d,2} - G^{d,1} + c}{T}.$$

We note that we tested different values for c, but that $c = 1$ appeared best able to capture the experimental glucose data. Recall that $G^{d,i}$ denotes the median pig glucose concentration at time t_i, and that $t_1 = 0$ minutes and $t_2 = 2$ minutes, as there was no measurement at time $T = 1$.

We utilize a normalized least-squares inspired cost functional which penalizes deviations from all three states (insulin, glucose, and glucagon). Specifically, we define

$$C(\theta) = C_I(\theta) + C_G(\theta) + C_{G_\ell}(\theta), \tag{3.3}$$

where

$$C_I(\theta) := \sum_{i=1}^{N} \left(\frac{I(t_i;\theta) - I^{d,i}}{I^{d,i}} \right)^2 \tag{3.4}$$

$$C_G(\theta) := \sum_{i=1}^{N} \left(\frac{G(t_i;\theta) - G^{d,i}}{G^{d,i}} \right)^2 \tag{3.5}$$

$$C_{G_\ell}(\theta) := \sum_{i=1}^{N} \left(\frac{G_\ell(t_i;\theta) - G_\ell^{d,i}}{G_\ell^{d,i}} \right)^2 \tag{3.6}$$

Here $I(t_i;\theta)$ denotes the solution of insulin in the IVGTT IGG system (Eqs (2.1), (3.2), and (2.3)) evaluated at time t_i, as a function of the model parameters θ; similar statements holds for $G(t_i,\theta)$ and $G_\ell(t_i,\theta)$. The parameter vector

$$\theta := (k_1, k_2, k_3, k_4, \delta_1, \delta_2, \delta_3, \delta_4, n, p, z, h)$$

is then estimated to minimize C, with respect to non-negativity constraints. The code was developed and executed in MATLAB 2022b using *fmincon* from the nonlinear optimization toolbox, and the ODE system was numerically solved with MATLAB's *ode23s*. All model simulations were performed with initial conditions, $G(0) = G^{d,1}$, $I(0) = I^{d,1}$, and $G_\ell(0) = G_\ell^{d,1}$.

Multi-start optimization was performed, and the initial parameter ranges utilized are provided in Table 2. We note that while the initial conditions for the optimization algorithm are contained in this range, the best fit parameter value may lie outside of it. To ensure that a global minimum was achieved, we repeated the optimization 1000 times while randomizing initial estimates between the ranges seen in Table 2. We used an 12-dimensional Sobol set (as $\theta \in \mathbb{R}^{12}$) transformed to the hypercube $[0, \gamma]^\rho$ where $\rho = 12$ is the length of the parameter vector θ and γ is the upper bound for each parameter value. During optimization, all parameter values were constrained to remain non-negative.

After the multi-start optimization was performed, we constructed tornado plots to ensure that we located the global minimum of the cost function. The tornado plots were generated by varying one parameter at a time within 5%, 10%, 15%, and 20% of its computed optimal value, and subsequently calculating the cost functional value. If a change in parameter value led to a decrease in the cost functional, the parameter value was changed accordingly, and the process was repeated until all local changes in parameter values led to only increases in the cost.

To quantify the uncertainty of the fitted parameters, we also fit the IGG model to individual pigs, and thus obtained a distribution for each model parameter. Individual pig data is provided in Figure 3, where we again utilized the same cost function (3.3) as with the median data. Fits to individual pigs are provided in Figure A7, and parameter distributions are shown in Figure A8. The mean ± standard deviation (SD) of each parameter are also reported in Table 2.

3.3. Insulin sensitivity and glucose effectiveness

One of the main applications of the minimal model is its ability to provide a patient's glucose effectiveness and insulin sensitivity to both aid in diagnosing a patient with type 2 diabetes, as well as understanding the severity of the disease [43, 44]. We now explore how to calculate both insulin sensitivity and glucose effectiveness using the IGG model. We utilize Bergman's definitions to calculate both glucose effectiveness and insulin sensitivity [45]. Glucose effectiveness (E) is defined as the rate of change of glucose with respect to current glucose levels:

$$E := -\frac{\partial \dot{G}}{\partial G}. \tag{3.7}$$

Here $\dot{G}$ is the rate of change of the plasma glucose concentration G, i.e., $\dot{G} = dG/dt$. Thus, glucose effectiveness for the IGG model is given by

$$E = (\delta_2 I + \delta_3). \tag{3.8}$$

Where I is the concentration of insulin.

Bergman also defines the insulin sensitivity (S) as the ability of insulin to stimulate glucose disappearance [45]. More precisely,

$$S := \frac{\partial E_{SS}}{\partial I_{SS}}, \tag{3.9}$$

where the subscript SS indicates that the quantities are measured at steady state. Using the above definition, the insulin sensitivity for the IGG model is therefore

$$S = \delta_2. \tag{3.10}$$

4. Results and discussion

4.1. Model captures in vivo data

The intravenous glucose tolerance test (IVGTT) data presented in Figure 3 reveals several interesting trends. First, we observe that glucose falls below basal levels, reaching a median near 2 mmol/L within the first 20–60 minutes after infusion. Within this same time period, glucagon peaks above basal levels, reaching a median high of 15 pmol/L. Prior to the dip in glucose, insulin reaches its highest level of about 0.6 μg/L. Insulin and glucose reach steady state levels within the first hour after glucose infusion; however, glucagon takes approximately twice as long to plateau. A primary goal was to examine how well the IGG model could reproduce these trends via parameter optimization. Prior to optimizing parameters, we have proven that the IGG model has a unique positive steady state, and have further discussed the stability of this steady state; see Appendix A.1 and A.2 for details.

We incorporated the median insulin, glucose, and glucagon data to estimate our model parameters via a multi-start optimization procedure. Minimization of a normalized least-squares inspired cost functional, defined as C in Eq (3.3), was performed; we note that cost function penalizes simultaneous deviations of all three model states (insulin, glucose and glucagon) from the data. More details about the optimization process are given in Subsection 3.2 of the Methods section, and MATLAB code may also be found on GitHub. Estimated parameter values are provided in Table 2, and Figure 4 shows tornado plots when individually varying each best fit parameter within 5%, 10%, 15%, and 20% of its original value. Note that varying each parameter does not lead to a decrease in the cost function C, providing evidence that we are likely at a global minimum. Estimated means and standard deviations for individual parameters are computed via fits to individual pigs; see Section A.6 and Figure A8.

The results, provided in Figure 5, demonstrate that our model is able to capture the median of the data well. Quantitatively, we compute an adjusted R^2 (R^2_{adj}) value of 0.9283, and the corresponding cost functional value of $C = 0.96976$ at the optimal parameters. Recall that R^2_{adj} incorporates model complexity (number of parameters), and will be used to compare the IGG model fit with other model fits below, which possess a different number of parameters; R^2_{adj} values closer to 1 generally indicate a better fit to data, and can be used to compare models with different degrees of complexity.

As discussed in Section 2, we also consider a two-state insulin-glucose model (see Eqs (A.17)–(A.18) in Section A.3 in the Appendix), which does not appear to capture the IVGTT data as well as the IGG model. Quantitatively, when fitting to only insulin and glucose data, we utilize an adjusted cost function $\bar{C}$, which excludes fitting to glucagon, and is defined in Eq (A.19). The $\bar{C}$ for the IGG fit provided in Figure 5 is 0.7847, while the corresponding measures for the insulin-glucose model are $R^2_{adj} = 0.7754$ and $\bar{C} = 1.2508$; see also Figure A2 for a visualization of the insulin-glucose model fit. We also fit the minimal model (Eqs (A.20)–(A.22)) introduced by Bergman to the same data set (see Section A.4 in the Appendix for a more detailed discussion of the minimal model). Figure 6 shows the result of the best fit of the minimal model to the same data set compared with the best fit for the

IGG model. As with the two-state insulin-glucose model, when estimating parameters in the minimal model, we consider the cost function $\bar{C}$ in Eq (A.19). We compute $R^2_{adj} = 0.77$ for the minimal model, while $R^2_{adj} = 0.9283$ for the IGG model, suggesting that the IGG model significantly improves on capturing the dynamics of the data when compared to the minimal model ($\bar{C} = 1.5016$ for the fit of the minimal model). The best fit parameter values and tornado plots for the minimal model can be found in Section A.4 in the Appendix (Table A2 and Figure A5, respectively).

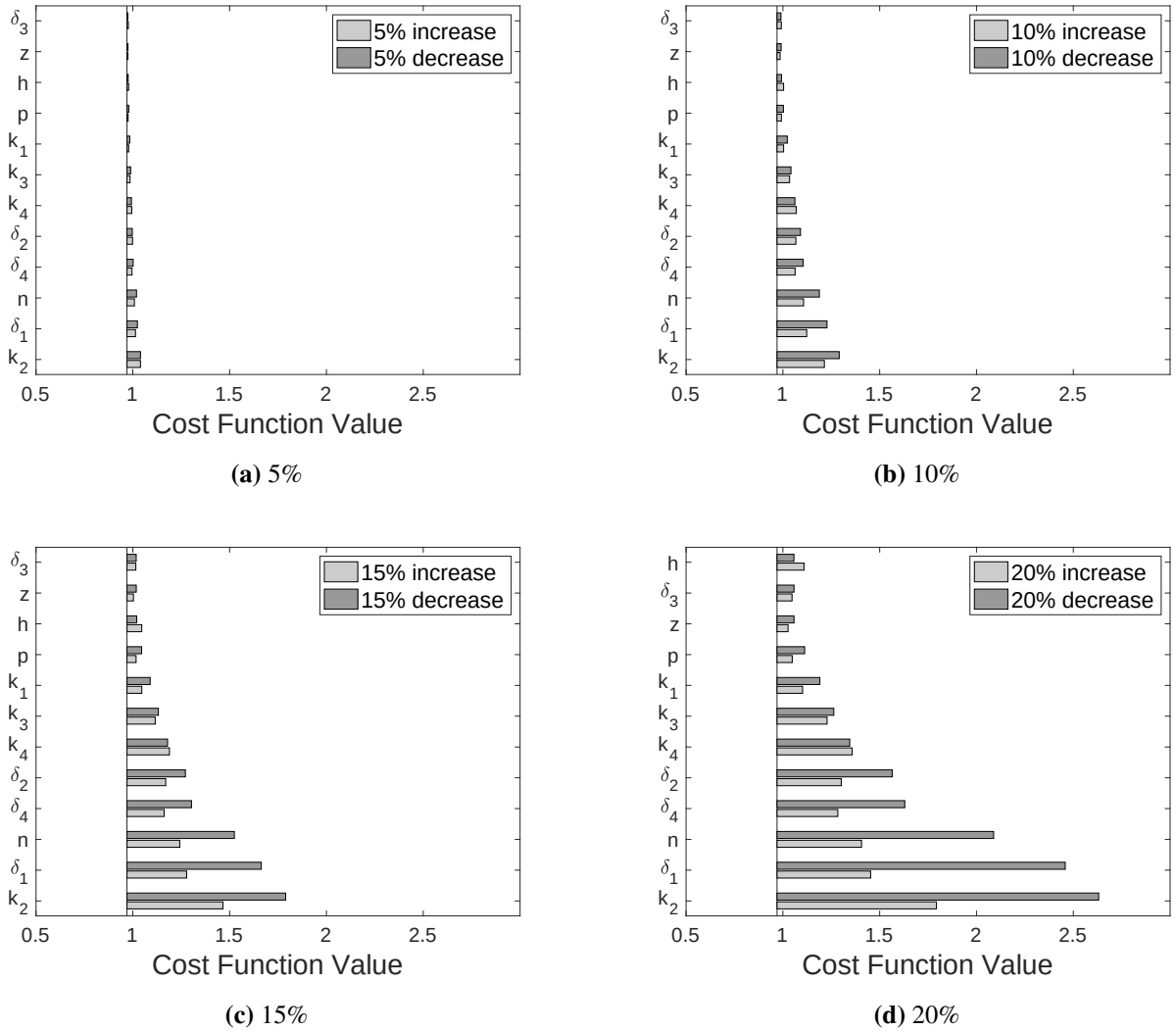

(a) 5%

(b) 10%

(c) 15%

(d) 20%

Figure 4. Validation of optimal parameters in IGG model. Tornado plots for the change in the cost function (C) when varying each parameter by the given percentage of its estimated optimal value. The vertical line represents the minimum residual. Parameter values changed by (a) 5%, (b) 10%, (c) 15% , and (d) 20%.

4.2. Estimated insulin sensitivity and glucose effectiveness

Referring to Section 3.3 and using the pre-dose value of insulin as the basal insulin concentration ($I^{d,1}$), we calculate the glucose effectiveness (E) for the estimated model parameters as

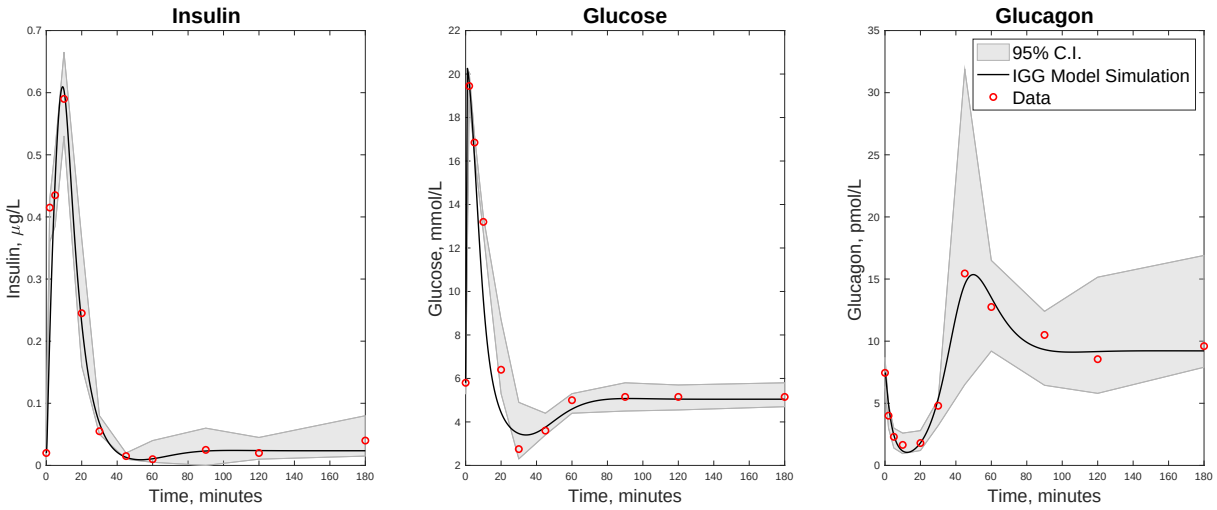

Figure 5. Fits of IGG model to data. The best fit for the IGG model. Here, the constant dosage $\bar{u} = 14.65$ was used with initial time $t_0 = 0$ and dose length $T = 1$ minute. The initial conditions for insulin, glucose, and glucagon were taken to be the initial values of the data. The cost functions evaluated at the optimal set of parameters are $C = 0.96976$ (insulin-glucose-glucagon cost) and $\bar{C} = 0.78407$ (insulin-glucose cost). See Table 2 for the corresponding estimated parameters. Left plot shows insulin profile, middle shows glucose profile, and right shows glucagon profile.

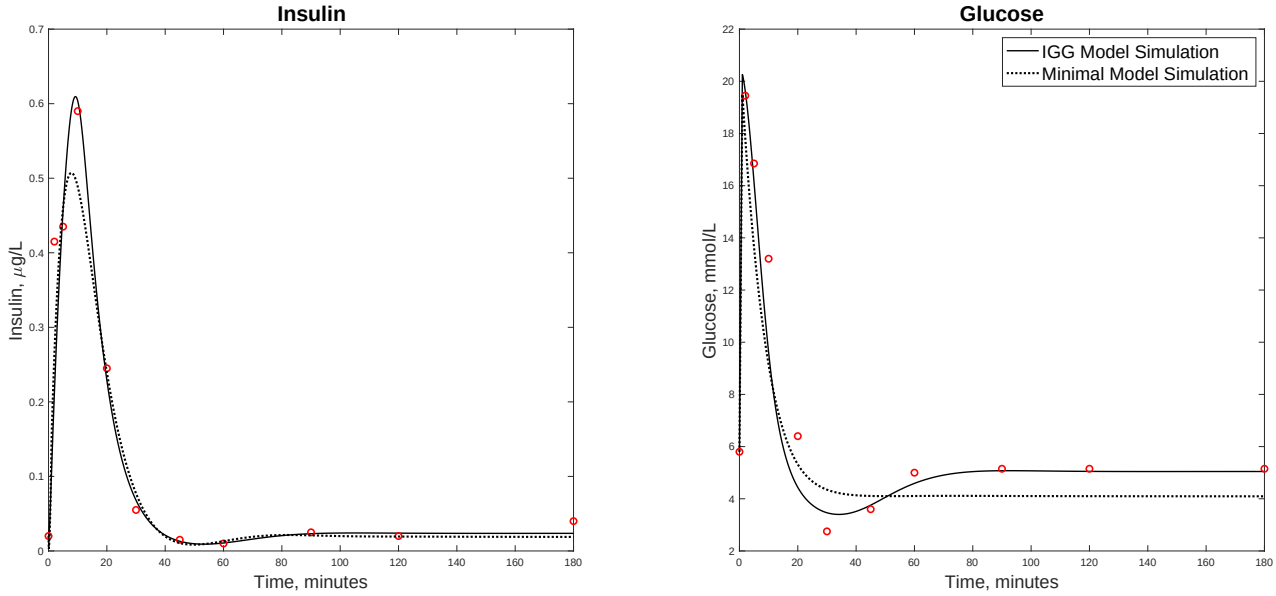

Figure 6. Comparison of model fits. The best fit for the minimal model (dashed line) together with the best fit of the IGG model (solid line); experimental medians are provided in red. The cost function at the given parameters for the minimal model fit is $\bar{C} = 1.5016$, with a corresponding R^2_{adj} value of 0.7569. Left is insulin profile and right is glucose profile.

Table 2. Table of initial estimate ranges, best fit parameter values when fitting the median of the pig data, mean and standard deviation when fitting individual pigs, and units for the IGG model, as well as the same (relevant) parameters utilized to simulate the dIGG model. When fitting, a multi-start method was utilized, and the initial range denotes the the interval for initializations.

Parameter	Initial range	Estimate (median data)	Mean ± SD (individual data)	Units
k_1	[0 2]	0.13	0.17 ± 0.06	$\frac{\mu g}{L \cdot min}$
k_2	[0 100]	9.81	9.06 ± 2.7	$\frac{mmol}{L}$
k_3	[0 2]	0.01	0.01 ± 0.01	$\frac{mmol}{pmol \cdot min}$
k_4	[0 2]	21.9	21.81 ± 5.39	$\frac{pmol}{L \cdot min}$
δ_1	[0 2]	0.13	0.20 ± 0.13	$\frac{1}{min}$
δ_2	[0 2]	0.17	0.14 ± 0.07	$\frac{L}{\mu g \cdot min}$
δ_3	[0 2]	0.01	0.02 ± 0.02	$\frac{1}{min}$
δ_4	[0 2]	0.35	0.38 ± 0.20	$\frac{1}{min}$
p	[0 10]	99.87	99.66 ± 1.38	$\frac{L}{\mu g}$
z	[0 10]	1.35	4.48 ± 6.13	$\frac{L}{mmol}$
h	[0 4]	2.45	3.14 ± 1.33	$\frac{mmol}{L}$
n	[0 10]	5.64	6.32 ± 2.6	-
t_0	-	0	-	min
T	-	1	-	min
$\bar{u}$	-	14.65	-	$\frac{mmol}{L}$

$E = 0.0134\,/\text{min}$ which is comparable to values for dogs, mice, humans, and rats reported in [46]. Moreover, it has been reported that insulin-independent clearance of glucose contributes to approximately 70% of glucose clearance, with the remainder occurring through the insulin-dependent pathway [46]. Here, at basal levels of insulin, we calculate that the insulin-independent clearance (δ_3) is approximately 70% of total glucose clearance ($\delta_3 + \delta_2 I^{d,1}$). This provides evidence that the calibrated IGG model mechanistically captures the dynamics of the insulin-glucose-glucagon regulatory system, at least with respect to the utilized data in [41].

Note that the insulin sensitivity factor is the slope of glucose effectiveness with respect to basal insulin values, and is relatively simple to interpret. Precisely, δ_2 controls the per-capita impact of insulin on glucose clearance, so that a high δ_2 value results in an increased clearance of glucose and indicates sensitivity to insulin, whereas a low δ_2 yields less clearance of glucose and indicates insulin resistance [47]. Our insulin sensitivity factor estimated by fitting the median of the pig data is $0.17 \frac{\text{L}}{\mu\text{g mins}}$. In [48], Bergman estimates insulin sensitivity factors between $0.0802 - 0.2674 \frac{\text{L}}{\mu\text{g mins}}$ (using the conversion factor $1\mu U = 0.0347\mu g$; [49]), indicating that our value lies within a biologically reasonable range. It is worth noting, however, that other reported ranges exist within which our estimation does not fall. To demonstrate the role of insulin sensitivity on glucose regulation, we simulated the dynamics of the IGG model for lower insulin sensitivities($\delta_2 = S < 0.0802$), which we term a "diseased" state, as it corresponds to a simplified

model of diabetes. As expected, we observed persistent elevated glucose levels which produce an increased peak in insulin production and a decreased peak in glucagon. The simulation results can be found in Section A.5 in the Appendix (Figure A6).

4.3. IGG dynamics in disease

In this section, we consider the dIGG model introduced in Section 2.2, where glucose feedback on insulin is removed, and hence insulin is considered as an external input. Recall that this system models diseases where insulin regulation is disrupted, such as insulin-dependent diabetes. To investigate how the removal of glucose feedback on insulin production impacts glucose and glucagon dynamics, we utilize the fitted insulin profile from Figure 5 as a baseline input $\hat{I}$, and perturb $\hat{I}$ to simulate simplified scenarios that occur in diabetes (specifically in insulin-dependent diabetes). We note that in the absence of any perturbation to the insulin profile $\hat{I}$, the solution to the dIGG model produces the dynamics observed in Figure 5 precisely, i.e., to the solution of the original IGG model system. Simple scale and delay perturbations to I are considered in Sections 4.3.1–4.3.3 to allow us to make direct comparisons to the non-diseased IGG dynamics (Figure 5), while direct insulin administration as a function of insulin half-life is considered in Section 4.3.4. We note that in simply perturbing baseline insulin profiles, we are ignoring physiological and pharmacokinetic considerations, which may be important in clinical applications. However, as our primary goal is to elucidate phenomenon using an idealized model, we believe such a study nevertheless provides mechanistic insight. Furthermore, similar methods are utilized frequently in mathematical models [50–52].

4.3.1. High glucose levels can reduce glucagon production in the near absence of insulin

We begin by simulating the dynamics of the dIGG models (2.4)–(2.5) when decreasing insulin secretion; specifically, we take the insulin profile from Figure 5 and reduce the total (integral) insulin concentration by 50%, which provides a new insulin profile $\hat{I}$ (solid line in left panel of Figure 7). Here, we aim to understand how inadequate insulin administration, which may occur due to a fear of hypoglycemia or incorrectly counting carbohydrates, impacts the dynamics of glucose and glucagon. We define $\hat{I}(t)$ as follows:

$$\hat{I}(t) = \frac{1}{2} \times I(t) \tag{4.1}$$

where I is the original insulin concentration.

Figure 7 shows the response of the dIGG model when the total external insulin concentration is reduced by 50%. We see that a reduction in insulin secretion leads to elevated glucose levels over time compared with the original insulin profile, with glucose levels remaining above 6 mmol/L. Moreover, we note that the glucose spike is relatively constant with respect to both models (approximately 20 mmol/L). On the other hand, we observe that glucagon has an increased minimum value compared to the original insulin profile and that the maximum of glucagon is significantly reduced.

The simulation of the reduced insulin profile yields several insights. First, the increased minimum value of glucagon while glucose levels remain elevated suggests that reduced insulin levels may lead to less glucagon suppression. More interestingly, despite lower levels of insulin, glucagon peaks at a

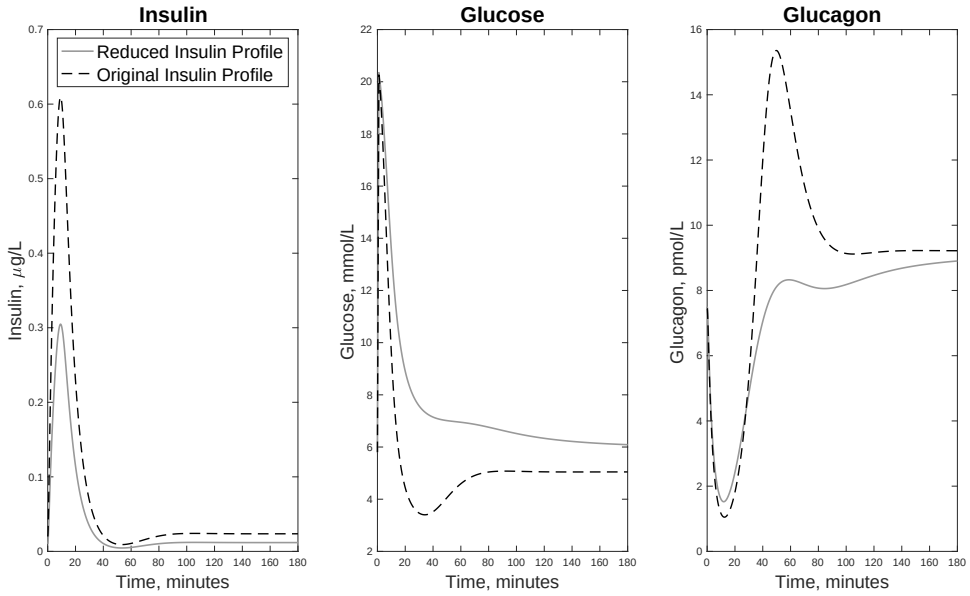

Figure 7. Dynamics of the dIGG models (2.4)–(2.5) when reducing the total (integral) insulin concentration from Figure 5 by 50% . Recall that in this model, there is no feedback of glucose on insulin production, and that $\hat{I}$ is given by (4.1). All other parameters, initial conditions, and dose u appearing in the dIGG model may be found in Table 2.

much lower value, suggesting that elevated glucose levels are able to significantly suppress glucagon. This is particularly interesting because while it has been documented that glucagon secretion depends on both insulin and glucose, the role each plays is not fully understood. The results in Figure 7 thus suggest that high glucose levels can greatly reduce glucagon production in the near absence of insulin. This demonstrates that the irregular patterns of glucagon secretion in type 2 diabetes (in particular, over secretion) may not be explained solely by the dysfunction of β cells (which secrete insulin), supporting research that has suggested that α cells (the glucagon-secreting cells) are also dysfunctional in type 2 diabetes [53–55].

4.3.2. Delayed insulin administration may increase the risk of hypoglycemia

As in the previous section, we aim to understand how suboptimal diabetes management may impact insulin and glucose dynamics by mimicking a delay in insulin administration after a glucose spike (e.g., delaying insulin administration after a large meal). Here, we investigate the dynamics of glucose and glucagon when the peak of insulin concentration is delayed. Here, we again consider the curve associated with the insulin profile in Figure 5, and delay the insulin dynamics by 20 minutes to produce the external signal $\hat{I}$ (i.e., we shift the insulin dynamics by 20 minutes; see the left panel of Figure 8). Here, we define $\hat{I}(t)$ as follows:

$$\hat{I}(t) = \begin{cases} I(0), & t \in [0, 20] \\ I(t-20), & t \in (20, 180] \end{cases}. \tag{4.2}$$

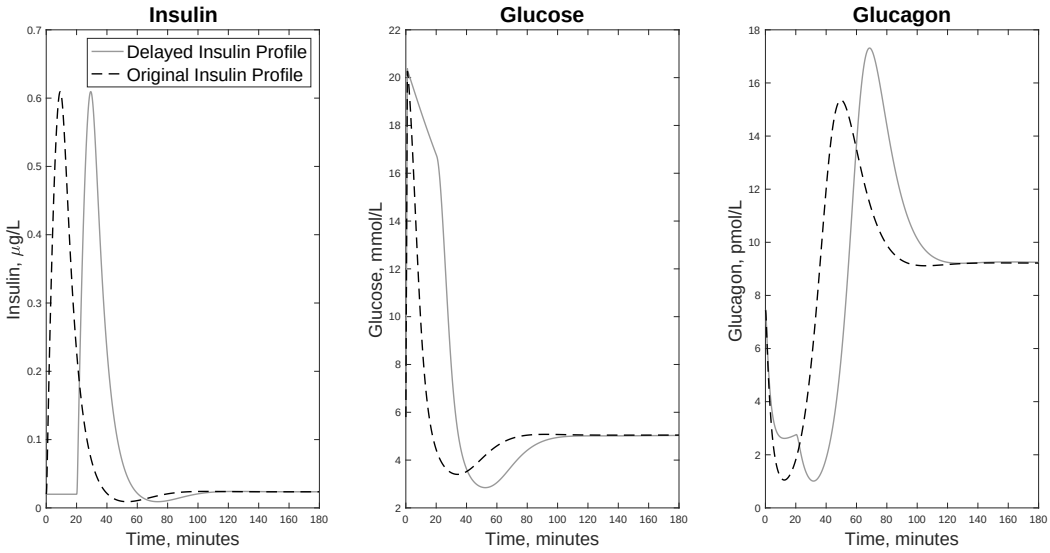

Figure 8. Dynamics of the dIGG model when shifting the insulin profile from Figure 5 by 20 minutes. Recall that in this system, there is no feedback of glucose on insulin, and that $\hat{I}$ is given by (4.2). All other parameters, initial conditions, and dose u appearing in the dIGG model may be found in Table 2.

Where I is the original insulin profile. Note that during the first 20 minutes, we fix the insulin concentration at its initial (assumed steady state) value.

First we note that by construction, there is no insulin in the first 20 minutes of the simulation. Despite this, both glucose and glucagon decrease during this period. This decrease in glucose levels, even in the absence of insulin, suggests that glucagon plays an important role in regulating glucose levels by reducing its production. Thus, glucagon has dual roles in the regulation of blood sugar: in both helping lower glucose levels, as well as its primary role in raising blood glucose.

Lastly, we note that glucose has a slightly lower minimum compared with the original insulin profile simulation. Furthermore, we see that glucagon dynamics remain below baseline (7.45 pmol/L) for a longer period of time compared with the original profile, about 60 minutes compared with 40 minutes for the non-delayed case. The slight decrease in glucose minimum suggests that delaying the insulin profile may lead to an increase in hypoglycemic risk due to the delayed suppression of the glucagon profile. Note however that glucose levels in the delayed insulin profile remain above 10 mmol/L, consistent with a hyperglycemic event, for around the first 40 minutes of the simulation.

4.3.3. When insulin administration is delayed, smaller amounts can reduce the risk of hypoglycemia

Figure 9 shows simulation results of the dIGG model when combining both a reduction (as in Section 4.3.1) and a delay (as in Section 4.3.2) of the insulin profile. We define $\hat{I}(t)$ as follows:

$$\hat{I}(t) = \begin{cases} I(0), & t \in [0, 20] \\ \frac{1}{2} \times I(t-20), & t \in (20, 180] \end{cases}. \tag{4.3}$$

where I is the original insulin profile. As in Section 4.3.2, we fix the insulin concentration in the first 20 minutes at the initial unperturbed insulin concentration.

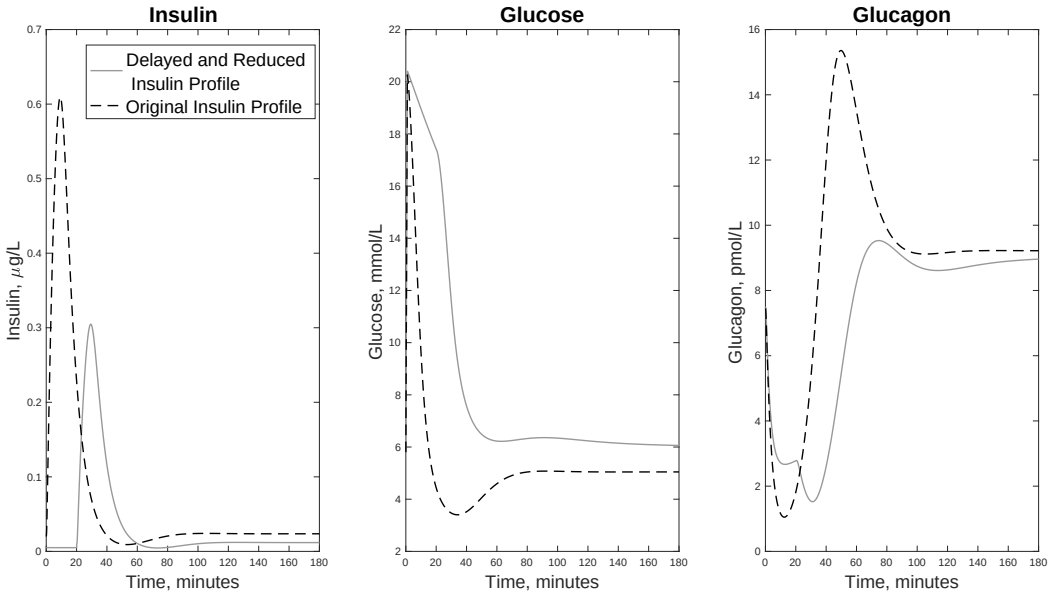

Figure 9. Dynamics of the dIGG model when both reducing and delaying the insulin profile from Figure 5 by 50% and 20 minutes, respectively. Recall that in this system, there is no feedback of glucose on insulin, and that $\hat{I}$ is given by (4.3). All other parameters, initial conditions, and dose u appearing in the dIGG model may be found in Table 2.

When compared with Figure 8, we see that in Figure 9 there is no severe hypoglycemic event. These results suggest that when insulin is administered later, less insulin may be needed to avoid hypoglycemic events. This has important applications in diabetes management, as continually monitoring the disease is difficult and late administrations are inevitable; thus, a late administration of insulin may require a reduction in the amount of insulin taken. However, we note that in Figure 9 we see that glucose levels remain above basal glucose levels (6 mmol/L) for the entirety of the 180 minutes whereas the original insulin profile returns to basal levels (and below basal levels) within approximately 20 minutes. Persistent high blood glucose levels are a critical concern in diabetes management, as they can lead to serious long-term health complications. Therefore, caution is needed when reducing insulin amounts after a missed/delayed insulin injection; while this may prevent a hypoglycemic event, it can contribute to harmful prolonged hyperglycemia.

In the IGG model, insulin and glucagon interact synergistically to regulate glucose levels. However, when feedback on insulin is removed, a time delay in insulin results in disruption to glucagon dynamics, and thus leads to impaired regulation of glucose. It has been documented that ill-timed insulin doses may result in an increased risk of hypoglycemia [56, 57]. Our simulations suggest that the reason for this is due to the peak of insulin no longer occurring at the same time as the peak of glucose and the minimum of glucagon.

4.3.4. Longer half-lives of exogenous insulin may increase the risk of hypoglycemic events

As a final application of the dIGG model, we consider the response of the system to doses of insulin with different half-lives. The aim of this is to more closely resemble difficulties that arise in

diabetes management, as insulins that are administered have a longer half-life compared to endogenous insulin [58]. We consider a simple exponentially decaying external insulin profile $\hat{I}$, with decay rate k and administered (constant) dosage U. The dose was assumed to be given at $t = 0.01$ minutes after the glucose injection, so that

$$\hat{I}(t) = \begin{cases} 0 & t \in [0, 0.01) \\ Ue^{-kt}, & t \in [0.01, 180] \end{cases} \tag{4.4}$$

Recall that the decay rate is related to the half-life τ via

$$k = \frac{\ln(2)}{\tau}. \tag{4.5}$$

The dose U was chosen to be the maximum change in the median insulin data, relative to the initial concentration, so as to mimic the endogenous insulin response upon glucose injection. That is, using the notation from Section 3.1,

$$U = \max_{i \in (1,n)} \left(I^{d,i} - I^{d,0} \right). \tag{4.6}$$

We considered three possible half-lives: 10 minutes to closely replicate endogenous insulin, 60 minutes to replicate a majority of mealtime FDA approved insulins, and 120 minutes to investigate the effects of longer-lasting insulin. Note here that insulin was taken to be an intravenous dose rather than a subcutaneous dose for simplicity (i.e., pharmocokinetics are ignored). The results are shown in Figure 10.

We observe that as the half-life of insulin increases, glucose levels significantly decrease when compared to the IGG insulin dynamics, and remain below 2 mmol/L at 180 minutes (compare to middle panel of Figure 5). Furthermore, as the half life of insulin is increased, the peak of glucagon is suppressed. In the case of the 120 minute half life, glucagon does not return to basal levels in the 180 minutes.

As the half-life of insulin increases, the response of glucagon to low blood glucose levels becomes significantly more impaired, which leads to longer and more severe hypoglycemia. The failure of glucagon to respond to low blood glucose levels in type 1 diabetes is well documented [9]. Our simulations thus suggest that a main cause of the lack of response of glucagon is due to the slower clearance of insulin. In the original simulations, we observe that insulin peaks and then decreases rapidly, allowing for glucagon to respond to lower blood glucose levels. However, in the case of exogenous insulin with longer half-lives, the reduction in insulin clearance means that glucagon is suppressed for longer and therefore cannot respond appropriately to low blood glucose levels as demonstrated in Figure 10. This also suggests that blood glucose levels may be more challenging to regulate in patients administering insulin, since if glucagon is not responding appropriately, a patient may no longer rely on the inhibition of glucagon to regulate glucose levels. This is especially clear from simulation of the "healthy" IGG model in Figure 5, where we observe that when glucose undershoots its steady state value, glucagon is able to rapidly regulate levels back to steady state. This demonstrates the degree to which the body relies on the anti-insulin properties of glucagon to regulate glucose levels, and highlights the importance of developing insulins that have half-lives closely resembling endogenous insulin in order to avoid impairing the function of glucagon and thus making diabetes management simpler.

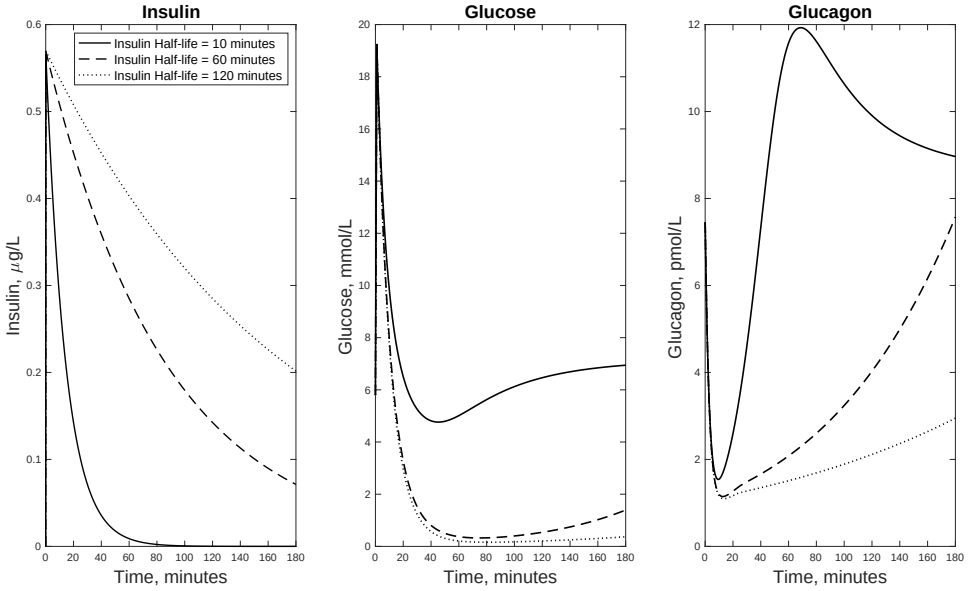

Figure 10. Dynamics of the dIGG model when varying the half-life of insulin. Half-lives of insulin are taken to be 10, 60, and 120 minutes. Recall $\hat{I}$ is given by (4.4). All other parameters, initial conditions, and dose u appearing in the dIGG model may be found in Table 2.

5. Conclusions

In this work we have developed a three-state model of insulin, glucose, and glucagon dynamics and validated our model by fitting it to the median of publicly available intravenous glucose tolerance test (IVGTT) pig data. Then, to better understand the system in a diabetic state, we removed the feedback of glucose on insulin production (see Figure 2), which allowed us to investigate the impact of the loss of regulation of insulin on glucose dynamics, and perhaps more interestingly, glucagon dynamics. This is a simplified phenomena of what occurs in insulin-dependent diabetes and helps shed light on possible complications in diabetes management.

Specifically, we have developed a simple mechanistic model of insulin-glucose-glucagon dynamics (IGG model) to aid in our understanding of glucose and glucagon response when using exogenous insulin. When glucose feedback on insulin production was removed (dIGG model), perturbations of the insulin profile from the endogenous response leads to impairment of glucagon response (Figures 7, 9 and 10); inhibition of glucagon subsequently leads to prolonged and severe hypoglycemia (Figures 8 and 10). Moreover, Figure 5 demonstrates the importance of the synergy between insulin and glucagon to optimally regulate glucose; we observed that an undershoot of the glucose steady state value is rapidly counteracted via glucagon, which is not observed in Figure 10, where feedback on insulin was removed. Upon the removal of feedback, we see that it is still possible for glucagon to regulate the system, but only if the insulin profile is adjusted (Figure 9), which highlights the important role of communication between glucagon and insulin to ensure that both are responding properly to glucose levels. However, for patients with diabetes, achieving insulin

regulation via external mechanisms similar to endogenous insulin secretion can be nearly impossible, and thus dysfunction of glucagon is often observed, further complicating diabetes management.

A major goal of this work is to present a simple model that is able to mechanistically capture IVGTT dynamics. Importantly, we do not claim that this model is necessarily appropriate to study all aspects of insulin-glucose dynamics, but rather that it provides insight into regulatory mechanisms which can be further investigated experimentally; our IGG and dIGG models also provide insights into short-term disease dynamics for those trying to externally control insulin secretion. Many other important models exist, including the discussed minimal model introduced by Bergman and colleagues [45, 48, 59, 60], which was influential in our inclusion of glucagon in the regulatory network. We emphasize that other physiologically-inspired models to describe the IVGTT have since been proposed, including those introduced by De Gaetano et al. [21, 26, 27] which include explicit time delays in insulin secretion in response to elevated glucose levels; extensions of such models continue to be developed and studied [28]. Delay models have proven very useful in understanding the long-term oscillatory behavior of insulin-glucose dynamics [14], and have even been extended to include the role of glucagon and the phenomenon of glucagon resistance [61]. We view the model presented here as complimentary to such approaches, in that we are interested in understanding the role of glucagon feedback on responses after a glucose spike (simulated through IVGTT) and the consequences of this feedback in diabetes management. We also note that our model does produce a time delay between the glucose and insulin peaks (approximately 8 minutes; see Figure 5), which thus provides a potential biological delay mechanism via glucagon. Lastly, our model is able to produce biphasic insulin release profiles, as the first insulin peak occurs approximately 8 minutes after the glucose spike, and the second peak occurs around 80 minutes later (Figure 5); the second peak is relatively small, but this is due to the calibration of the model to the IVGTT pig data, and is not a feature of the model itself (for example, see Pig 6 in Figure A7 for a more noticeable second peak). Hence the model has the ability to capture both insulin peaks, but will need to be tested using data with a more pronounced second peak to assess fidelity. Of course, understanding the phases of insulin is important, but it is not the main focus of the work presented here, as we are primarily interested in investigating how alterations in the administration of exogenous insulin influence glucose regulation.

Future work will continue to focus on the deregulation of insulin. We intend to use the proposed IGG models (2.1)–(2.3) to understand how the progression of type 1 diabetes impacts this system by explicitly incorporating an autoimmune response and thus β cell loss as in [62], but with the dynamics of glucagon explicitly modeled. We will then combine this model to the insulin-glucose regulatory system via insulin (i.e., decreased β cell mass implies reduced insulin secretion) to understand how insulin, glucose, and glucagon become increasingly deregulated throughout the progression of the disease. Other possible research directions include investigating more complex interactions in glucose regulation, such as ability of α cells to increase glucagon production in low glucose regimes [63]; in our current model, glucose levels above a threshold always inhibit glucagon production. Indeed, the inclusion of such mechanisms may yield more pronounced, or even different, observations with respect to exogenous insulin dosing and diabetes management, and hence provide testable hypotheses which can be experimentally analyzed. Lastly, in this work we have worked exclusively with data from healthy animal subjects, and hypothesized about the effect of feedback deregulation on glucagon and glycemic control using an idealized model variation (the dIGG model); in future work, we plan to extend the model and utilize experimental data for human (from IVGTT data) and diabetic subjects

(e.g. diabetic pigs, as in [64]), as well incorporate data from scenarios with exogenous insulin injections (as in [65]). Indeed, such extensions will determine the overall clinical significance of our model. For example, one natural extension may be to incorporate an explicit delay between insulin production and glucose level. In this case, the right-hand side of dI/dt in (2.1) would be replaced with $k_1 G^n(t-\tau)/(k_2^n + G^n(t-\tau))$, where τ is a fixed time delay modeling the response of additional sensing and signaling which precedes insulin secretion by β cells . Such an extension would naturally allow the model to capture ultradian oscillations [66], since delay differential equations often exhibit periodic behavior, as discussed in the previous paragraph. Such extensions could then allow the model-based personalization of glucose tolerance and regulatory capacity from IVGTT data, with translation to predicting hypoglycemia risk and optimizing insulin/glucagon interventions in disease.

Data availability

MATLAB code for all figures and simulations presented in this work can be found at the following public GitHub repository: https://github.com/kenziealyse/IG-Paper.

Use of AI tools declaration

The authors declare they have not used Artificial Intelligence (AI) tools in the creation of this article.

Conflict of interest

The authors declare there is no conflict of interest.

References

1. B. Giri, S. Dey, T. Das, M. Sarkar, J. Banerjee, S. K. Dash, Chronic hyperglycemia mediated physiological alteration and metabolic distortion leads to organ dysfunction, infection, cancer progression and other pathophysiological consequences: An update on glucose toxicity, *Biomed. Pharmacotherapy.*, **107** (2018), 306–328. https://doi.org/10.1016/j.biopha.2018.07.157
2. M. Mouri, M. Badireddy, Hyperglycemia, in *StatPearls [Internet]*, StatPearls Publishing, 2023.
3. D. R. Wasag, J. W. Gregory, C. Dayan, J. N. Harvey, Excess all-cause mortality before age 30 in childhood onset type 1 diabetes: Data from the brecon group cohort in wales, *Arch. Dis. Child.*, **103** (2018), 44–48. https://doi.org/10.1136/archdischild-2016-312581
4. S. A. Amiel, The consequences of hypoglycaemia, *Diabetologia*, **64** (2021), 963–970. https://doi.org/10.1007/s00125-020-05366-3
5. G. Da Silva Xavier, The cells of the islets of langerhans, *J. Clin. Med.*, **7** (2018), 54. https://doi.org/10.3390/jcm7030054
6. P. V. Röder, B. Wu, Y. Liu, W. Han, Pancreatic regulation of glucose homeostasis, *Exp. Mol. Med.*, **48** (2016), e219. https://doi.org/10.1038/emm.2016.6
7. M. S. Rahman, K. S. Hossain, S. Das, S. Kundu, E. O. Adegoke, M. A. Rahman, et al., Role of insulin in health and disease: An update, *Int. J. Mol. Sci.*, **22** (2021), 6403. https://doi.org/10.3390/ijms22126403

8. B. A. Cooperberg, P. E. Cryer, Insulin reciprocally regulates glucagon secretion in humans, *Diabetes*, **59** (2010), 2936–2940. https://doi.org/10.2337/db10-0728
9. M. Bisgaard Bengtsen, N. Møller, Mini-review: Glucagon responses in type 1 diabetes–A matter of complexity, *Physiol. Rep.*, **9** (2021), e15009. https://doi.org/10.14814/phy2.15009
10. R. J. McCrimmon, R. S. Sherwin, Hypoglycemia in type 1 diabetes, *Diabetes*, **59** (2010), 2333–2339. https://doi.org/10.2337/db10-0103
11. R. N. Bergman, Origins and history of the minimal model of glucose regulation, *Front. Endocrinol.*, **11** (2021), 583016. https://doi.org/10.3389/fendo.2020.583016
12. P. Palumbo, S. Ditlevsen, A. Bertuzzi, A. De Gaetano, Mathematical modeling of the glucose–insulin system: A review, *Math. Biosci.*, **244** (2013), 69–81. https://doi.org/10.1016/j.mbs.2013.05.006
13. V. Subramanian, J. I. Bagger, J. J. Holst, F. K. Knop, T. Vilsbøll, A glucose-insulin-glucagon coupled model of the isoglycemic intravenous glucose infusion experiment, *Front. Physiol.*, **13** (2022), 911616. https://doi.org/10.3389/fphys.2022.911616
14. B. Huard, G. Kirkham, Mathematical modelling of glucose dynamics, *Curr. Opin. Endocr. Metab. Res.*, **25** (2022), 100379. https://doi.org/10.1016/j.coemr.2022.100379
15. M. Lombarte, M. Lupo, G. Campetelli, M. Basualdo, A. Rigalli, Mathematical model of glucose–insulin homeostasis in healthy rats, *Math. Biosci.*, **245** (2013), 269–277. https://doi.org/10.1016/j.mbs.2013.07.017
16. I. Garzilli, S. Itzkovitz, Design principles of the paradoxical feedback between pancreatic alpha and beta cells, *Sci. Rep.*, **8** (2018), 10694. https://doi.org/10.1038/s41598-018-29084-4
17. S. Sangeetha, C. Sreepradha, S. Sobana, P. Bidisha, R. C. Panda, Modeling and control of the glucose-insulin-glucagon system in type i diabetis mellitus, *ChemBioEng Rev.*, **7** (2020), 89–100. https://doi.org/10.1002/cben.201900015
18. R. A. Kelly, M. J. Fitches, S. D. Webb, S. Pop, S. J. Chidlow, Modelling the effects of glucagon during glucose tolerance testing, *Theor. Biol. Med. Model.*, **16** (2019), 21. https://doi.org/10.1186/s12976-019-0115-3
19. A. Emami, J. El Youssef, R. Rabasa-Lhoret, J. Pineau, J. R. Castle, A. Haidar, Modeling glucagon action in patients with type 1 diabetes, *IEEE J. Biomed. Health Inf.*, **21** (2016), 1163–1171. https://doi.org/10.1109/JBHI.2016.2593630
20. C. L. Adams, D. G. Lasseigne, An extensible mathematical model of glucose metabolism. part i: The basic glucose-insulin-glucagon model, basal conditions and basic dynamics, *Lett. Biomath.*, **5** (2018), 70–90. https://doi.org/10.1080/23737867.2018.1429332
21. A. De Gaetano, O. Arino, Mathematical modelling of the intravenous glucose tolerance test, *J. Math. Biol.*, **40** (2000), 136–168. https://doi.org/10.1007/s002850050007
22. M. F. Tabassum, M. Farman, P. A. Naik, A. Ahmad, A. S. Ahmad, S. M. Hassan, Modeling and simulation of glucose insulin glucagon algorithm for artificial pancreas to control the diabetes mellitus, *Network Model. Anal. Health Inf. Bioinf.*, **10** (2021), 42. https://doi.org/10.1007/s13721-021-00316-4

23. M. Watts, J. Ha, O. Kimchi, A. Sherman, Paracrine regulation of glucagon secretion: the $\beta/\alpha/\delta$ model, *Am. J. Physiol. Endocrinol. Metab.*, **310** (2016), E597–E611. https://doi.org/10.1152/ajpendo.00415.2015

24. M. Morettini, L. Burattini, C. Göbl, G. Pacini, B. Ahrén, A. Tura, Mathematical model of glucagon kinetics for the assessment of insulin-mediated glucagon inhibition during an oral glucose tolerance test, *Front. Endocrinol.*, **12** (2021), 611147. https://doi.org/10.3389/fendo.2021.611147

25. J. Sturis, K. S. Polonsky, E. Mosekilde, E. Van Cauter, Computer model for mechanisms underlying ultradian oscillations of insulin and glucose, *Am. J. Physiol.*, **260** (1991), E801–E809. https://doi.org/10.1152/ajpendo.1991.260.5.E801

26. S. Panunzi, P. Palumbo, A. de Gaetano, A discrete single delay model for the intra-venous glucose tolerance test, *Theor. Biol. Med. Modell.*, **4** (2007), 35. https://doi.org/10.1186/1742-4682-4-35

27. J. Li, M. Wang, A. De Gaetano, P. Palumbo, S. Panunzi, The range of time delay and the global stability of the equilibrium for an ivgtt model, *Math. Biosci.*, **235** (2012), 128–137. https://doi.org/10.1016/j.mbs.2011.11.005

28. J. Jin, J. Li, R. Xu, L. Yu, Z. Jin, A novel ivgtt model including interstitial insulin, *Math. Appl. Sci. Eng.*, **4** (2023), 12–29. https://doi.org/10.5206/mase/15505

29. J. Li, Y. Kuang, C. C. Mason, Modeling the glucose–insulin regulatory system and ultradian insulin secretory oscillations with two explicit time delays, *J. Theor. Biol.*, **242** (2006), 722–735. https://doi.org/10.1016/j.jtbi.2006.04.002

30. J. Li, Y. Kuang, Analysis of a model of the glucose-insulin regulatory system with two delays, *SIAM J. Appl. Math.*, **67** (2007), 757–776. https://doi.org/10.1137/050634001

31. D. S. Glass, X. Jin, I. H. Riedel-Kruse, Nonlinear delay differential equations and their application to modeling biological network motifs, *Nat. Commun.*, **12** (2021), 1788. https://doi.org/10.1038/s41467-021-21700-8

32. Z. Fu, E. R. Gilbert, D. Liu, Regulation of insulin synthesis and secretion and pancreatic beta-cell dysfunction in diabetes, *Curr. Diabetes Rev.*, **9** (2013), 25–53.

33. P. D. Docherty, J. G. Chase, C. E. Hann, T. F. Lotz, J. Lin, K. A. McAuley, et al., The identification of insulin saturation effects during the dynamic insulin sensitivity test, *Open Med. Inform. J.*, **4** (2010), 141–148. https://doi.org/10.2174/1874431101004010141

34. P. Ebeling, H. A. Koistinen, V. A. Koivisto, Insulin-independent glucose transport regulates insulin sensitivity, *FEBS Lett.*, **436** (1998), 301–303. https://doi.org/10.1016/s0014-5793(98)01149-1

35. I. Rix, C. Nexøe-Larsen, N. C. Bergmann, A. Lund, F. K. Knop, *Glucagon Physiology*, MDText.com, Inc., South Dartmouth (MA), 2000.

36. I. Quesada, E. Tudurí, C. Ripoll, A. Nadal, Physiology of the pancreatic α-cell and glucagon secretion: role in glucose homeostasis and diabetes, *J. Endocrinol.*, **199** (2008), 5–19. https://doi.org/10.1677/JOE-08-0290

37. D. Kawamori, A. J. Kurpad, J. Hu, C. W. Liew, J. L. Shih, E. L. Ford, et al., Insulin signaling in α cells modulates glucagon secretion in vivo, *Cell Metab.*, **9** (2009), 350–361. https://doi.org/10.1016/j.cmet.2009.02.007

38. J. Liljenquist, G. Mueller, A. Cherrington, U. Keller, J. Chiasson, J. Perry, et al., Evidence for an important role of glucagon in the regulation of hepatic glucose production in normal man., *J. Clin. Invest.*, **59** (1977), 369–374. https://doi.org/10.1172/JCI108649

39. F. Piccinini, R. N. Bergman, The measurement of insulin clearance, *Diabetes Care*, **43** (2020), 2296–2302. https://doi.org/10.2337/dc20-0750

40. F. P. Alford, S. Bloom, J. Nabarro, Glucagon metabolism in man. studies on the metabolic clearance rate and the plasma acute disappearance time of glucagon in normal and diabetic subjects, *J. Clin. Endocrinol. Metab.*, **42** (1976), 830–838. https://doi.org/10.1210/jcem-42-5-830

41. E. Manell, P. Hedenqvist, A. Svensson, M. Jensen-Waern, Establishment of a refined oral glucose tolerance test in pigs, and assessment of insulin, glucagon and glucagon-like peptide-1 responses, *PloS One*, **11** (2016), e0148896. https://doi.org/10.1371/journal.pone.0148896

42. A. R. Henderson, The bootstrap: A technique for data-driven statistics. using computer-intensive analyses to explore experimental data, *Clin. Chim. Acta*, **359** (2005), 1–26. https://doi.org/10.1016/j.cccn.2005.04.002

43. R. N. Bergman, Toward physiological understanding of glucose tolerance: Minimal-model approach, *Diabetes*, **38** (1989), 1512–1527. https://doi.org/10.2337/diab.38.12.1512

44. A. G. Gallardo-Hernández, M. A. González-Olvera, M. Castellanos-Fuentes, J. Escobar, C. Revilla-Monsalve, A. L. Hernandez-Perez, R. Leder, Minimally-invasive and efficient method to accurately fit the bergman minimal model to diabetes type 2, *Cell. Mol. Bioeng.*, **15** (2022), 267–279. https://doi.org/10.1007/s12195-022-00719-x

45. R. N. Bergman, Y. Z. Ider, C. R. Bowden, C. Cobelli, Quantitative estimation of insulin sensitivity., *Am. J. Physiol.*, **236** (1979), E667. https://doi.org/10.1152/ajpendo.1979.236.6.E667

46. B. Ahrén, G. Pacini, Glucose effectiveness: Lessons from studies on insulin-independent glucose clearance in mice, *J. Diabetes Investig.*, **12** (2021), 675–685. https://doi.org/10.1111/jdi.13446

47. E. Ferrannini, A. Mari, How to measure insulin sensitivity, *J. Hypertension.*, **16** (1998), 895–906. https://doi.org/10.1097/00004872-199816070-00001

48. R. N. Bergman, L. S. Phillips, C. Cobelli, Physiologic evaluation of factors controlling glucose tolerance in man: Measurement of insulin sensitivity and beta-cell glucose sensitivity from the response to intravenous glucose., *J. Clin. Invest.*, **68** (1981), 1456–1467. https://doi.org/10.1172/jci110398

49. J. L. Knopp, L. Holder-Pearson, J. G. Chase, Insulin units and conversion factors: A story of truth, boots, and faster half-truths, *J. Diabetes Sci. Technol.*, **13** (2019), 597–600. https://doi.org/10.1177/1932296818805074

50. H. Wang, J. Li, Y. Kuang, Mathematical modeling and qualitative analysis of insulin therapies, *Math. Biosci.*, **210** (2007), 17–33. https://doi.org/10.1016/j.mbs.2007.05.008

51. H. Wang, J. Li, Y. Kuang, Enhanced modelling of the glucose–insulin system and its applications in insulin therapies, *J. Biol. Dyn.*, **3** (2009), 22–38. https://doi.org/10.1080/17513750802101927

52. X. Song, M. Huang, J. Li, Modeling impulsive insulin delivery in insulin pump with time delays, *SIAM J. Appl. Math.*, **74** (2014), 1763–1785. https://doi.org/10.1137/130933137

53. N. Honzawa, K. Fujimoto, T. Kitamura, Cell autonomous dysfunction and insulin resistance in pancreatic α cells, *Int. J. Mol. Sci.*, **20** (2019), 3699. https://doi.org/10.3390/ijms20153699

54. J. S. Moon, K. C. Won, Pancreatic α-cell dysfunction in type 2 diabetes: Old kids on the block, *Diabetes Metab. J.*, **39** (2015), 1–9. https://doi.org/10.4093/dmj.2015.39.1.1

55. S. K. Venugopal, P. Sankar, I. Jialal, *Physiology, Glucagon*, StatPearls Publishing, 2023.

56. S. Robinson, R. S. Newson, B. Liao, T. Kennedy-Martin, T. Battelino, Missed and mistimed insulin doses in people with diabetes: A systematic literature review, *Diabetes Technol. Ther.*, **23** (2021), 844–856. https://doi.org/10.1089/dia.2021.0164

57. A. Petznick, Insulin management of type 2 diabetes mellitus, *Am. Fami. Physician*, **84** (2011), 183–190.

58. A. D. Sanlioglu, H. A. Altunbas, M. K. Balci, T. S. Griffith, S. Sanlioglu, Clinical utility of insulin and insulin analogs, *Islets*, **5** (2013), 67–78. https://doi.org/10.4161/isl.24590

59. R. N. Bergman, Minimal model: Perspective from 2005, *Horm. Res.*, **64** (2006), 8–15.

60. R. N. Bergman, Origins and history of the minimal model of glucose regulation, *Front. Endocrinol.*, **11** (2021), 583016. https://doi.org/10.3389/fendo.2020.583016

61. R. B. Cohen, J. Li, A novel model and its analysis on the metabolic regulations of glucose, insulin, and glucagon, *SIAM J. Appl. Math.*, **81** (2021), 2684–2703. https://doi.org/10.1137/21M1390876

62. B. Topp, K. Promislow, G. Devries, R. M. Miura, D. T Finegood, A model of β-cell mass, insulin, and glucose kinetics: Pathways to diabetes, *J. Theor. Biol.*, **206** (2000), 605–619. https://doi.org/10.1006/jtbi.2000.2150

63. M. Watts, A. Sherman, Modeling the pancreatic α-cell: Dual mechanisms of glucose suppression of glucagon secretion, *Biophys. J.*, **106** (2014), 741–751. https://doi.org/10.1016/j.bpj.2013.11.4504

64. M. Izumi, K. Hano, T. Kato, A. Hirata, P. Thaw, A. Seki, et al., Glucose and insulin responses following streptozotocin administration for the induction of a type 1 diabetes mellitus model in microminipig, *J. Vet. Med. Sci.*, **87** (2025), 1122–1127. https://doi.org/10.1292/jvms.25-0145

65. N. A. Qinna, A. A. Badwan, Impact of streptozotocin on altering normal glucose homeostasis during insulin testing in diabetic rats compared to normoglycemic rats, *Drug Des. Devel. Ther.*, 2515–2525. https://doi.org/10.2147/DDDT.S79885

66. C. Simon, G. Brandenberger, Ultradian oscillations of insulin secretion in humans, *Diabetes*, **51** (2002), S258–S261. https://doi.org/10.2337/diabetes.51.2007.s258

67. F. R. Gantmakher, *The Theory of Matrices*, American Mathematical Soc., 2000.

68. N. Wu, G. An, A quantitative systems pharmacology model of the incretin hormones gip and glp1, glucagon, glucose, insulin, and the small molecule dpp-4 inhibitor, linagliptin, *J. Pharm. Sci.*, **113** (2024), 278–289. https://doi.org/10.1016/j.xphs.2023.09.006

Appendix

A.1. Uniqueness of steady state of IGG model

In this section, we show that systems (2.1)–(2.3) has a unique positive steady state (i.e., a steady state in $\mathbb{R}^3_{>0}$). Let $(I_*, G_*, G_{\ell,*})$ denote a steady state of systems (2.1)–(2.3). Thus, $(I_*, G_*, G_{\ell,*})$ satisfy the following system of equations:

$$\frac{k_1 G_*^n}{k_2^n + G_*^n} - \delta_1 I_* = 0 \tag{A.1}$$

$$k_3 G_{\ell,*} - (\delta_2 I_* + \delta_3) G_* = 0 \tag{A.2}$$

$$\frac{k_4}{1 + z(G_* - h)^+ + pI_*} - \delta_4 G_{\ell,*} = 0 \tag{A.3}$$

Equation (A.1) implies that

$$I_* = f_1(G_*), \tag{A.4}$$

where

$$f_1(G_*) := \frac{k_1}{\delta_1} \cdot \frac{G_*^n}{k_2^n + G_*^n}. \tag{A.5}$$

Solving (A.2) for $G_{\ell,*}$, and using $I_* = f_1(G_*)$ yields

$$\begin{aligned} G_{\ell,*} &= \frac{\delta_2 f_1(G_*) + \delta_3}{k_3} G_* \\ &=: f_2(G_*). \end{aligned} \tag{A.6}$$

Define

$$\begin{aligned} f_3(G_*) &:= z(G_* - h)^+ + pI_* \\ &= z(G_* - h)^+ + p f_1(G_*). \end{aligned} \tag{A.7}$$

Thus, Eq (A.3) can be written entirely in terms of G_*:

$$\frac{k_4/\delta_4}{1 + f_3(G_*)} - f_2(G_*) = 0. \tag{A.8}$$

Since $f_3(G_*)$ is increasing and $f_3(0) = 0$, the first term on the left-hand side of (A.8) is decreasing (as a function of G_*) and takes the value k_4/δ_4 at $G_* = 0$. The second term, $f_2(G_*)$ is increasing and satisfies $f_2(0) = 0$. Thus, Eq (A.8) has precisely one positive solution G_*. As $G_{\ell,*}$ and I_* are determined uniquely from f_2 and f_1, respectively, and are also strictly positive (if G_* is), the claim is shown: systems (2.1)–(2.3) has a unique positive steady state.

A.2. Stability of unique positive steady state of IGG model

As demonstrated in Section A.1, systems (2.1)–(2.3) possesses a unique positive steady state; note however by the analysis presented in that section, it is challenging to find an explicit expression for the positive equilibrium $(I_*, G_*, G_{\ell,*})$, as (A.8) is essentially a polynomial of degree $n+1$ in G_*. Nevertheless, we are interested in the dynamics of this nonlinear system of ODEs, and specifically in the stability of the steady state. To address local stability, we utilize the Routh-Hurtwitz stability criterion [67], as discussed below.

For simplicity, we introduce the following notation:

$$\begin{aligned} s_* &:= \delta_2 I_* + \delta_3 \\ D_* &:= 1 + z(G_* - h)^+ + pI_* \\ a_* &:= \frac{\partial}{\partial G}\left(\frac{k_1 G^n}{k_2^n + G^n}\right)\Big|_{G=G_*} = nk_1 k_2^n \frac{G_*^{n-1}}{(k_2^n + G_*^n)^2} \\ b_* &:= \frac{k_4 p}{D_*^2} \\ c_* &:= \frac{k_4 z}{D_*^2} \mathbb{1}_{\{G>h\}}(G_*). \end{aligned} \tag{A.9}$$

Here $\mathbb{1}_{\{G>h\}}(G_*)$ denotes the indicator function of the set $\{G_* \,|\, G_* > h\}$ evaluated at G_*, which arises due to differentiation of the right-hand side of (2.3) with respect to G, when computing the Jacobian at the equilibrium $(I_*, G_*, G_{\ell,*})$ (below). Note that non-differentiability of the vector field will occur if $G_* = h$, but as this does not appear to be the case in simulations (for example, $h = 2.45$ mmol/L for the model fit, while $G_* \approx 5.3$ mmol/L), so we ignore this case in the analysis presented here. All parameters defined above are non-negative, and are in fact strictly positive, with the possible exception of c_*, which may be zero if $G_* \le h$.

With the above notation, the Jacobian J_* evaluated at $(I_*, G_*, G_{\ell,*})$ is given by

$$J_* = \begin{pmatrix} -\delta_1 & a_* & 0 \\ -\delta_2 G_* & -s_* & k_3 \\ -b_* & -c_* & -\delta_4 \end{pmatrix}. \tag{A.10}$$

The characteristic polynomial of (A.10) can then be calculated. Let

$$\begin{aligned} X_* &:= \delta_2 G_* a_* \\ Y_* &:= k_3 c_* \\ Z_* &:= a_* b_* k_3. \end{aligned} \tag{A.11}$$

As with the previously introduced quantities, the above terms are nonnegative, so that all negative terms are explicitly labeled as such. With these definitions, the desired characteristic polynomial can be shown to be

$$p_{J_*}(\lambda) = \lambda^3 + A_1\lambda^2 + A_2\lambda + A_3, \tag{A.12}$$

where

$$\begin{aligned} A_1 &:= \delta_1 + \delta_4 + s_* \\ A_2 &:= \delta_1 s_* + \delta_4(\delta_1 + s_*) + X_* + Y_* \\ A_3 &= \delta_1\delta_4 s_* + \delta_4 X_* + \delta_1 Y_* + Z_*. \end{aligned} \tag{A.13}$$

For a three-dimensional system, the necessary and sufficient Routh-Hurwitz conditions for the equilibrium $(I_*, G_*, G_{\ell,*})$ to be locally asymptotically stable (i.e., for all three eigenvalues to have negative real parts) is for all of the coefficients to have the same sign, and for

$$\Delta := A_1 A_2 - A_3 \tag{A.14}$$

to be positive. Clearly $A_1, A_2, A_3 > 0$, so that the only nontrivial condition is $\Delta > 0$. Using the above definitions, Δ can be shown to be given by

$$\Delta = (\delta_1 + \delta_4)(\delta_1 + s_*)(\delta_4 + s_*) + (\delta_1 + s_*)X_* + (\delta_4 + s_*)Y_* - Z_*. \tag{A.15}$$

The above expression for Δ can be clearly interpreted with respect to stability; recall that (local) stability occurs when $\Delta > 0$, so that positive terms act to stabilize the system. The first term $(\delta_1 + \delta_4)(\delta_1 + s_*)(\delta_4 + s_*)$ involves decay only (recall that s_* is the net glucose clearance rate), and hence acts to stabilize the system. The next two terms correspond to the closed loop subsystems involving two species. Specifically, the first term $(\delta_1 + s_*)X_*$ corresponds to the glucose-insulin loop, and is also stabilizing: glucose stimulates insulin production via a_* in $X_* = a_*\delta_2 G_*$, while insulin mediates glucose removal via $\delta_2 G_*$, and $\delta_1 + s_*$ is the net decay rate in this loop (insulin and glucose). In this closed loop subsystem, the dynamics are completely stabilizing, and thus this term acts to increase Δ. A similar analysis can be made for $(\delta_4 + s_*)Y_*$ with respect to the glucose-glucagon closed loop subsystem: recall that $Y_* = k_3 c_*$, where c_* represents the repression of glucose on glucagon production, while k_3 quantifies the production of glucose as a function of glucagon levels, and $\delta_1 + s_*$ represents the combined glucagon and glucose decay. As in the previous subsystem, the closed loop interaction dynamics between glucagon and glucose are stabilizing, and hence this term increases Δ.

For the $Z_* = a_* b_* k_3$ term in Δ, we first note that in systems (2.1)–(2.3), there exists exactly one three node closed loop subsystem, which takes the form

$$G \xrightarrow{a_*} I \xrightarrow{b_*} G_\ell \xrightarrow{k_3} G. \tag{A.16}$$

More precisely, glucose stimulates insulin production (a_*), insulin suppresses the rate of glucagon production (b_*), and glucagon produces glucose (k_3). The gain through this negative feedback loop is precisely Z_*, which contains no damping terms, and hence measures how strongly a perturbation in glucose affects glucose levels after one full loop through the subsystem. It is thus destabilizing, since over-corrections to increases in glucose may lead to oscillatory behavior, precisely when Z_* is larger than the other (stabilizing) terms appearing in (A.15).

The data utilized in this work (see, e.g., Figure 3) appears to exhibit stability for the steady state $(I_*, G_*, G_{\ell,*})$, which is confirmed by the model fitting performed as discussed in Sections 3.2 and 4.1. Indeed, for the the ranges of individually fit parameters presented in Table 2 (column "Mean ± SD from individual fits"), numerically testing all $2^{\#\text{parameters}} = 2^{12}$ corners of the 12 dimensional hyper-rectangle, we observe that $\Delta > 0$ at all corners, which implies that the steady state is locally stable. We note that global stability is not guaranteed by the above analysis, and appears to be non-trivial to prove; however we do conjecture that $(I_*, G_*, G_{\ell,*})$ is globally asymptotically stable in the first octant when $\Delta > 0$. As it is not the primary focus of this work, we do not pursue this analysis further. When stability of $(I_*, G_*, G_{\ell,*})$ is lost, numerical evidence suggests that a Hopf bifurcation occurs when Δ becomes negative, and that a stable periodic orbit (in the first octant) arises. As an example, the parameter set

$(k_1, k_2, k_3, k_4, \delta_1, \delta_2, \delta_3, \delta_4, p, z, h, n) = (0.29, 5, 0.01, 64, 0.04, 0.14, 0.02, 0.08, 2000, 4, 3, 20)$ yields the approximate equilibrium $(I_*, G_*, G_{\ell,*}) \approx (0.039, 3.85, 9.78)$, with $\Delta \approx -3.8 \times 10^{-4}$ and corresponding eigenvalues of J_* are $\lambda_1 \approx -0.156$, $\lambda_{2,3} \approx 0.0054 \pm 0.11i$, i.e., one stable eigenvalue, with an unstable complex conjugate pair. Numerically, we observe a stable periodic limit cycle, as expected.

Lastly, although we do not provide a complete investigation of all parameters on model dynamics, a primary novelty of (2.1)–(2.3) is the inclusion of glucagon, and specifically the suppression of its production by glucose (via parameter z) and insulin (via parameter p); we thus briefly discuss their role in regulation. Note that increasing p or z strengthens the suppression of glucagon production, thereby reducing $G_{\ell,*}$ and hence G_* and I_*, which can be seen from the equations defining the steady state in Section A.1. From the analysis presented in this section on local stability, we observe contradictory effects of both p and z on stability. For example, recall the destabilizing loop gain $Z_* = a_* b_* k_3$ in Δ, with $b_* = k_4 p / D_*^2$, where $D_* \sim pI_*$. For small p, $b_* \approx 0$, and the equilibrium is stable. However, as p increases, b_* increases, and hence the steady state may become unstable if $\Delta < 0$. However, as p increases further, suppression saturates, and $b_* \sim 1/p$, which promotes stability. We note that this analysis is only heuristic, and for any precise conclusions, we would need to understand the relative importance of p and z with respect to other parameters, as well as their effect on the equilibrium concentrations (recall that we do not have explicit expressions for I_*, G_*, or $G_{\ell,*}$). As this is not the main focus of this work, we do not investigate these interactions further.

A.3. Two-state model

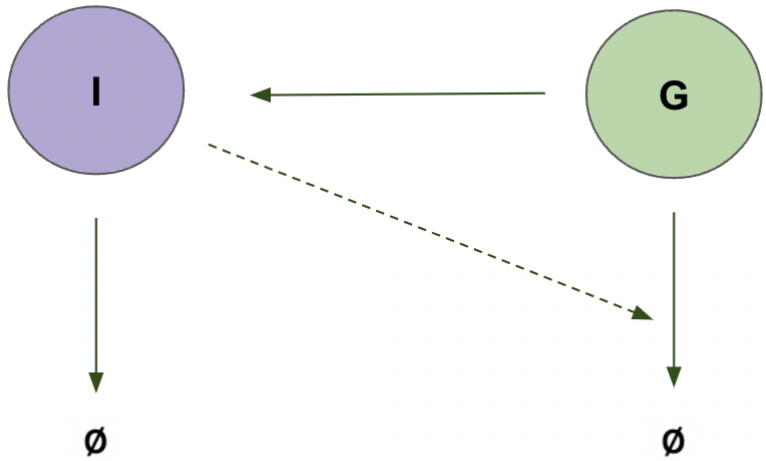

Figure A1. Schematic representing the interactions in the two-state insulin-glucose model. G denotes the glucose concentration, and I the insulin concentration.

Here we propose a two state model of insulin-glucose dynamics; see Section 2 for the rationale for utilizing the specific expressions in the below system of differential equations.

$$\frac{dI}{dt} = \frac{k_1 G^n}{k_2^n + G^n} - \delta_1 I \tag{A.17}$$

$$\frac{dG}{dt} = k_3 - (\delta_2 I + \delta_3)G \tag{A.18}$$

A schematic of the modeled interactions is provided in Figure A1. Note that in systems (A.17)–(A.18) we do not incorporate the role of glucagon on stimulating glucose production, and thus there is no inhibition of glucose or insulin in this system (compare to Eq (2.3)).

The results of fitting the insulin and glucose pig data to systems (A.17)–(A.18) are provided in Figure A2. We note that when calibrating the insulin-glucose model to the same data set, glucagon is not explicitly considered, and thus the following analogous cost functional is utilized:

$$\bar{C}(\theta) = C_I(\theta) + C_G(\theta), \tag{A.19}$$

where $\theta = (k_1, k_2, k_3, \delta_1, \delta_2, \delta_3, n)$ for the insulin-glucose model. For details on the external data and calibration methods, see Section 3. Tornado plots to ensure minimality are provided in Figure A3, and the optimal set of parameter values are shown in Table A1.

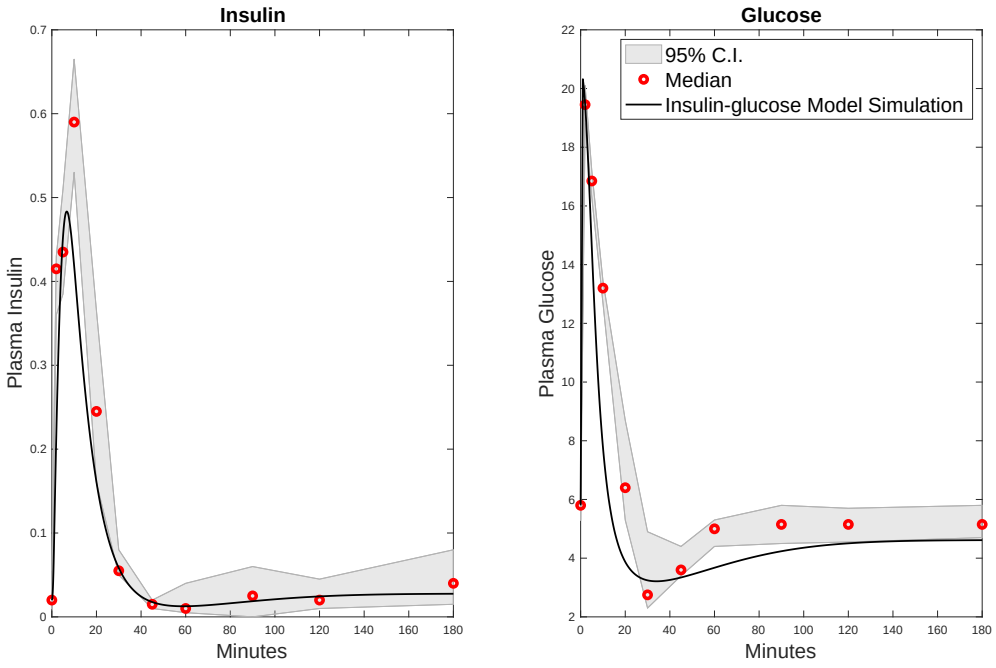

Figure A2. The best fit for the insulin-glucose models (A.17)–(A.18). The cost function evaluated at the optimal estimated parameter set is $\bar{C} = 1.2508$, and the corresponding R^2_{adj} value is 0.7754. See Table A1 for the corresponding estimated parameters.

A.4. A description of the minimal model

For completeness, we briefly summarize Bergman's minimal model here, and we refer the interested reader to [48] for more details. The minimal model consists of three states: insulin (I), glucose (G), and remote insulin (X). Here, insulin does not directly inhibit glucose; rather insulin enters a remote compartment (X) and X acts to inhibit glucose. Insulin production is a function of both time and the

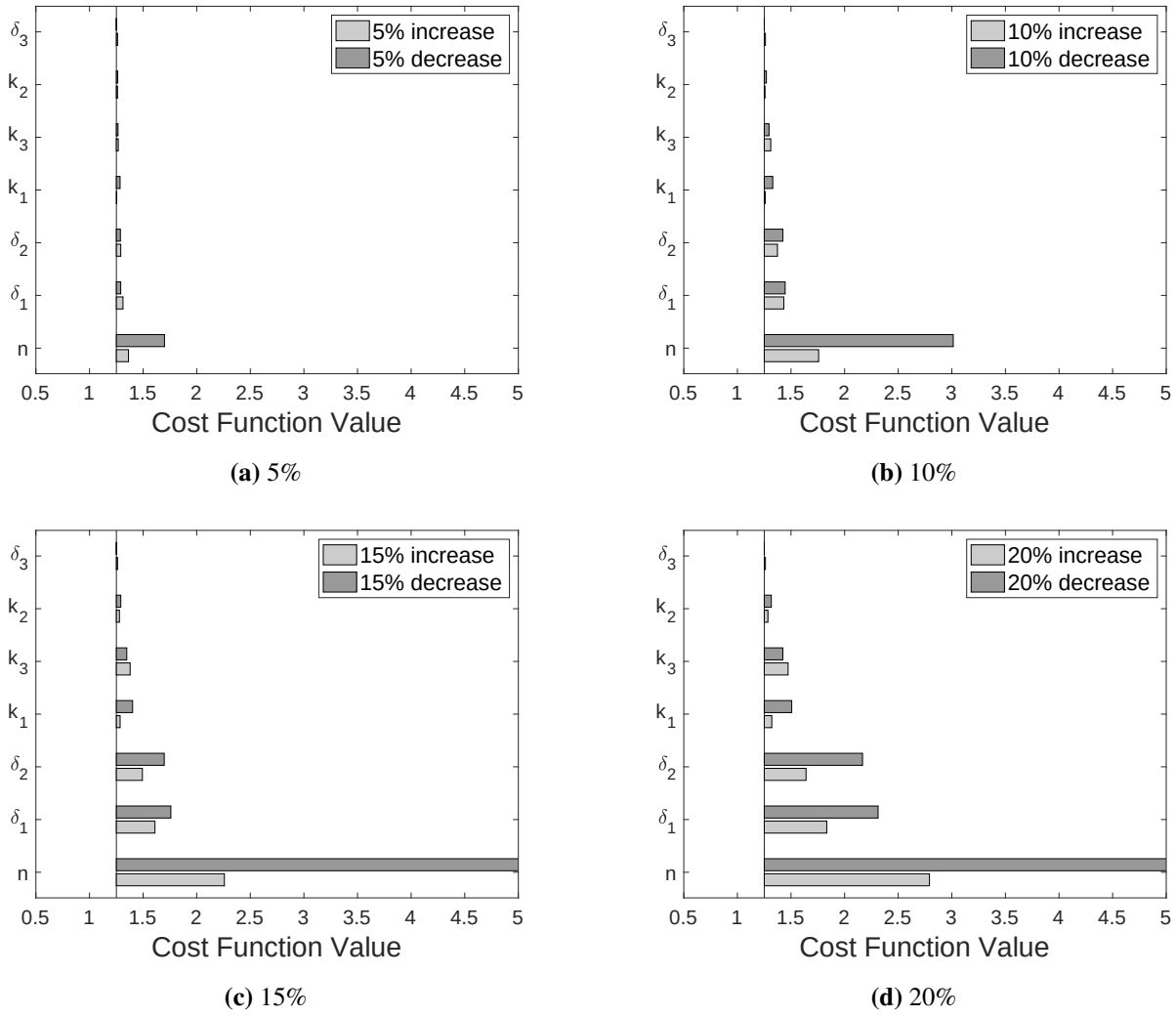

(a) 5% **(b)** 10%

(c) 15% **(d)** 20%

Figure A3. Validation of optimal parameters in the insulin-glucose two-state model. Tornado plots for the change in cost function ($\bar{C}$) when varying each parameter by the given percentage of its optimal value. The vertical line represents the minimum residual. Parameter values are changed by (a) 5%, (b) 10%, (c) 15%, and (d) 20%.

degree to which glucose exceeds a baseline threshold value h. Glucose production is constant with respect to a baseline level of glucose, which is dependent on the specific data set. More precisely, G_b is taken to be the initial value of glucose prior to the start of the IVGTT. The production of remote insulin is dependent on I, and glucose uptake occurs through both an insulin dependent and independent pathway. Lastly, both insulin and remote insulin have natural decay rates n and P_2, respectively. The ODEs utilized to describe these dynamics are defined below:

$$\frac{dI}{dt} = \gamma(G-h)^{+}t - nI \tag{A.20}$$

$$\frac{dG}{dt} = P_1 G_b - (P_1 + X)G \tag{A.21}$$

Table A1. Table of initial estimate ranges, best fit parameter values, and units for the insulin-glucose model (A.17)–(A.18).

Parameter	Initial range	Estimate	Units
k_1	[0, 1]	0.22	$\frac{\mu g}{L \cdot mins}$
k_2	[0, 1]	11640	$\frac{mmol}{L}$
k_3	[0, 1]	0.04	$\frac{mmol}{L \cdot mins}$
δ_1	[0, 1]	0.11	$\frac{1}{mins}$
δ_2	[0, 10]	0.28	$\frac{L}{\mu g \cdot mins}$
δ_3	[0, 2]	0.0001	$\frac{1}{mins}$
n	[0, 1]	3.36	-

$$\frac{dX}{dt} = P_3 I - P_2 X \tag{A.22}$$

Note that parameter labels do not correspond to parameters in the models introduced in Section 2, but are chosen to be consistent with [48]. We provide the best fit solution (Figure A4), estimated parameters (Table A2), and tornado plots (Figure A5) for the minimal models (A.20)–(A.22); recall that since glucagon is not considered in the minimal model, we use the cost function given by Eq (A.19) for parameter estimation, and that the parameter vector θ is defined as $\theta = (\gamma, h, n, P_1, P_2, P_3, G_b)$. For details on the external data and calibration methods, see Section 3. A comparison between the IGG model and the minimal model is provided in Figure 6 in the main text of the article.

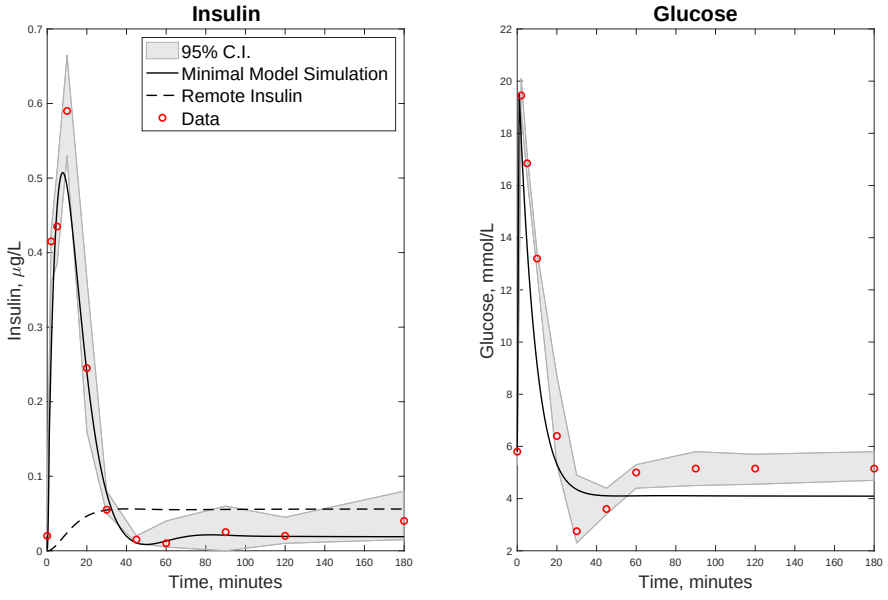

Figure A4. The best fit for the minimal models (A.20)–(A.22). The cost function evaluated at the optimal set of parameters is $\bar{C} = 1.5016$, and the adjusted R^2 value is $R^2_{adj} = 0.77$. See Table A2 for the corresponding estimated parameters.

Table A2. Table of initial estimate ranges, best fit parameter values, and units for the minimal models (A.20)–(A.22). Recall that G_b is not estimated, but instead is fixed as the initial value of glucose prior to the start of the IVGTT.

Parameter	Initial range	Estimate	Units
γ	[0, 1]	0.32	$\frac{\mu g}{mmol \cdot mins^2}$
h	[0, 1]	4.08	$\frac{mmol}{L}$
n	[0, 1]	33.44	$\frac{1}{mins}$
P_1	[0, 1]	0.13	$\frac{1}{mins}$
P_2	[0, 10]	0.002	$\frac{1}{mins}$
P_3	[0, 2]	0.24	$\frac{L}{\mu g mins^2}$
G_b	-	-	$\frac{mmol}{L}$

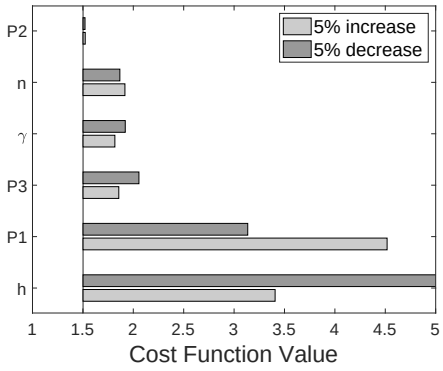

(a) 5%

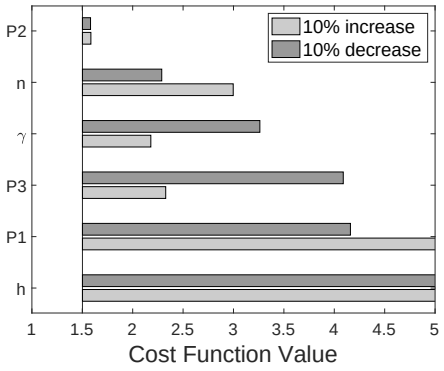

(b) 10%

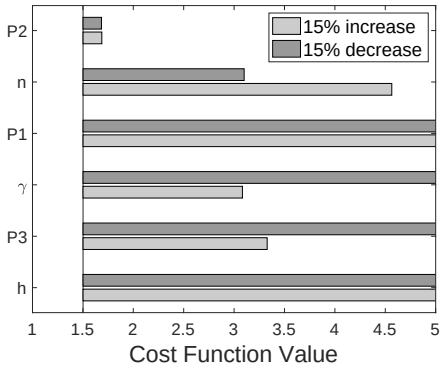

(c) 15%

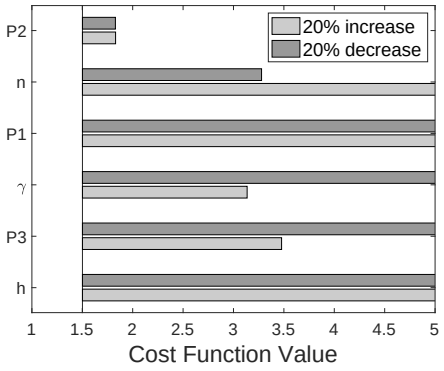

(d) 20%

Figure A5. Validation of optimal parameters in the minimal model. Tornado plots for the change in cost function ($\bar{C}$) when varying each parameter by the given percentage of its optimal value. The vertical line represents the minimum residual. Parameter values are changed by (a) 5%, (b) 10%, (c) 15%, and (d) 20%.

A.5. Insulin sensitivity in a healthy versus diseased state

Here we explore the impact of the insulin sensitivity factor S (as discussed in Section 4.2) in a simplified model of diabetes. Recall that this corresponds to a decrease in $S = \delta_2$ in the IGG model. A simulation is provided in Figure A6, where we observe both an increased spike in insulin production, a slower response to elevated glucose levels, and suppressed glucagon concentrations in the diseased case, when comparing to the response of the healthy state.

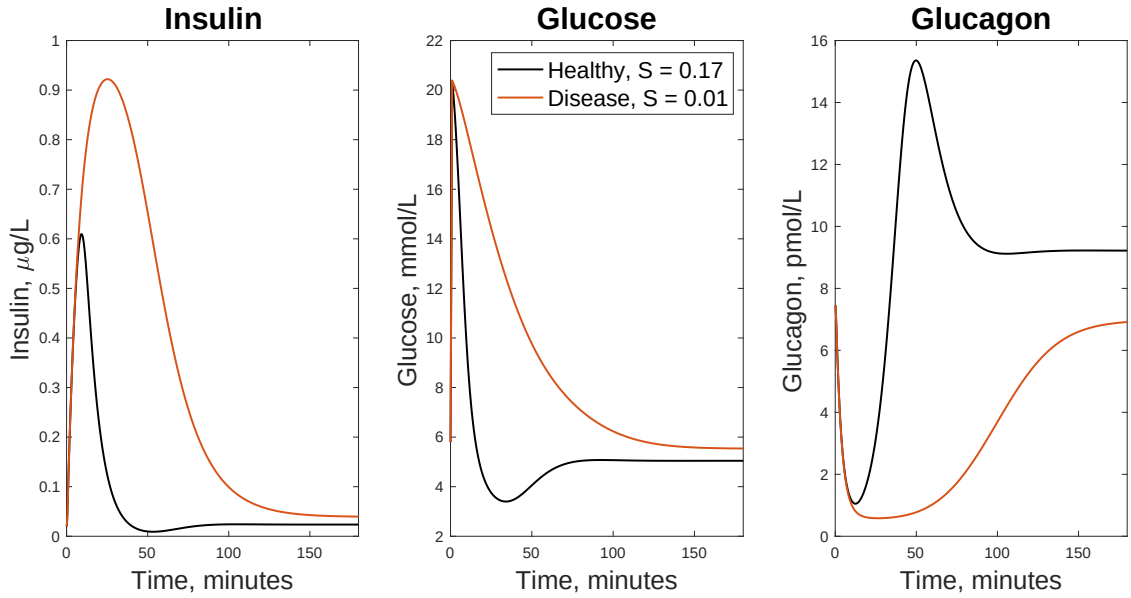

Figure A6. Simulation results when insulin sensitivity is in a healthy ($S = 0.17$) and diseased ($S = 0.01$) state. All other parameters, initial conditions, and dose u were identical to the simulation provided in Figure 5.

A.6. Fitting to individual pigs

We attempt to quantify the uncertainty in the parameter estimates for the IGG model by fitting the model to the data from the ten pigs individually (Figure 3), as opposed to the population median values at each time; thus we obtain distributions of the parameter values in Table 2 for the IGG model. We note that data from pigs 2, 3, 4 and 6 have no missing or zero values, the latter of which would yield an undefined cost function (3.3). Pigs 8, 9, and 10 are missing a glucagon value at the last time, and hence we ignore this time for glucagon in these pigs. Pigs 1, 5, and 7 have insulin value(s) that equal zero, so we ignore these data points for insulin in the cost C. For all fits, we utilized *fmincon* in MATLAB's 2022b nonlinear optimization toolbox. The fitting results are provided in Figure A7. We then looked at the distribution of parameter values for the 10 new sets of parameters from the 10 fitted pigs relative to the best fit parameter set from fitting the median of the pig data; the distributions for each parameter in the IGG model are provided in Figure A8. Means and standard deviations provided in Table 2 are computed using the distributions provided here.

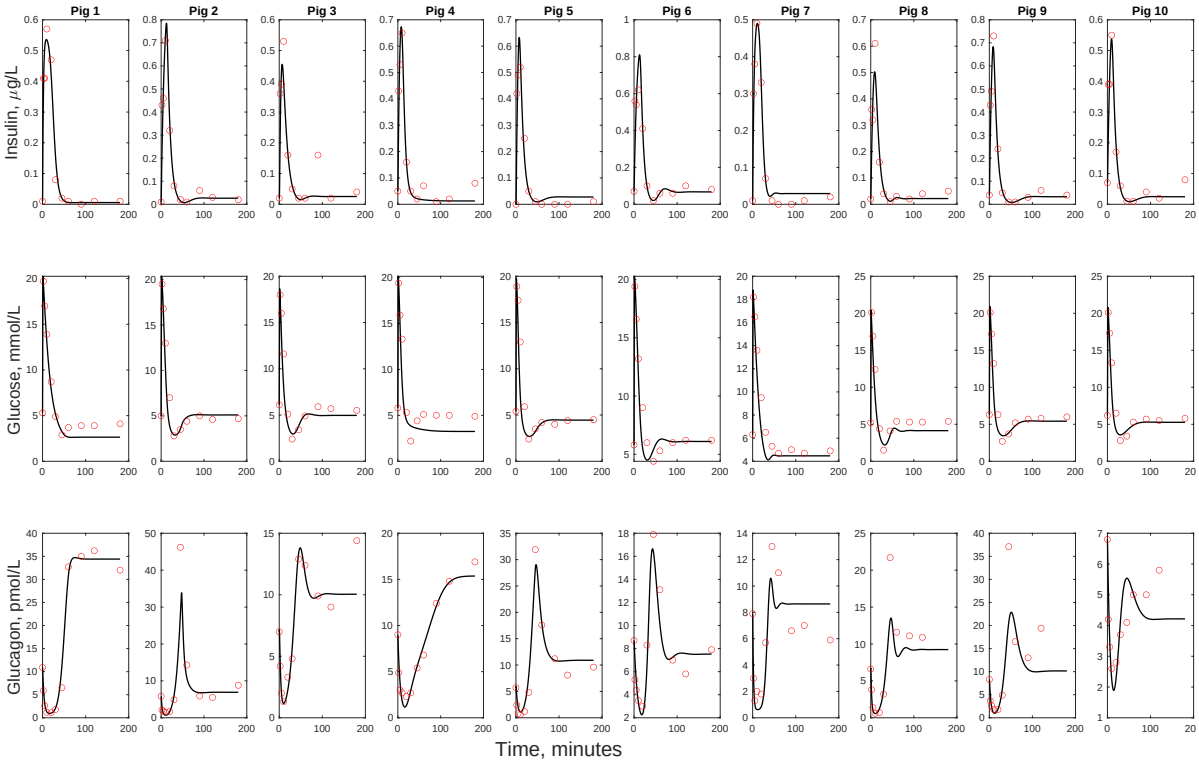

Figure A7. Model fits for individual pigs. The constant dosage $\bar{u}$ was adjusted accordingly for each pig and was applied at initial time $t_0 = 0$ for a time length of $T = 1$. The initial conditions for insulin, glucose, and glucagon were taken to be the initial values of the data for each pig.

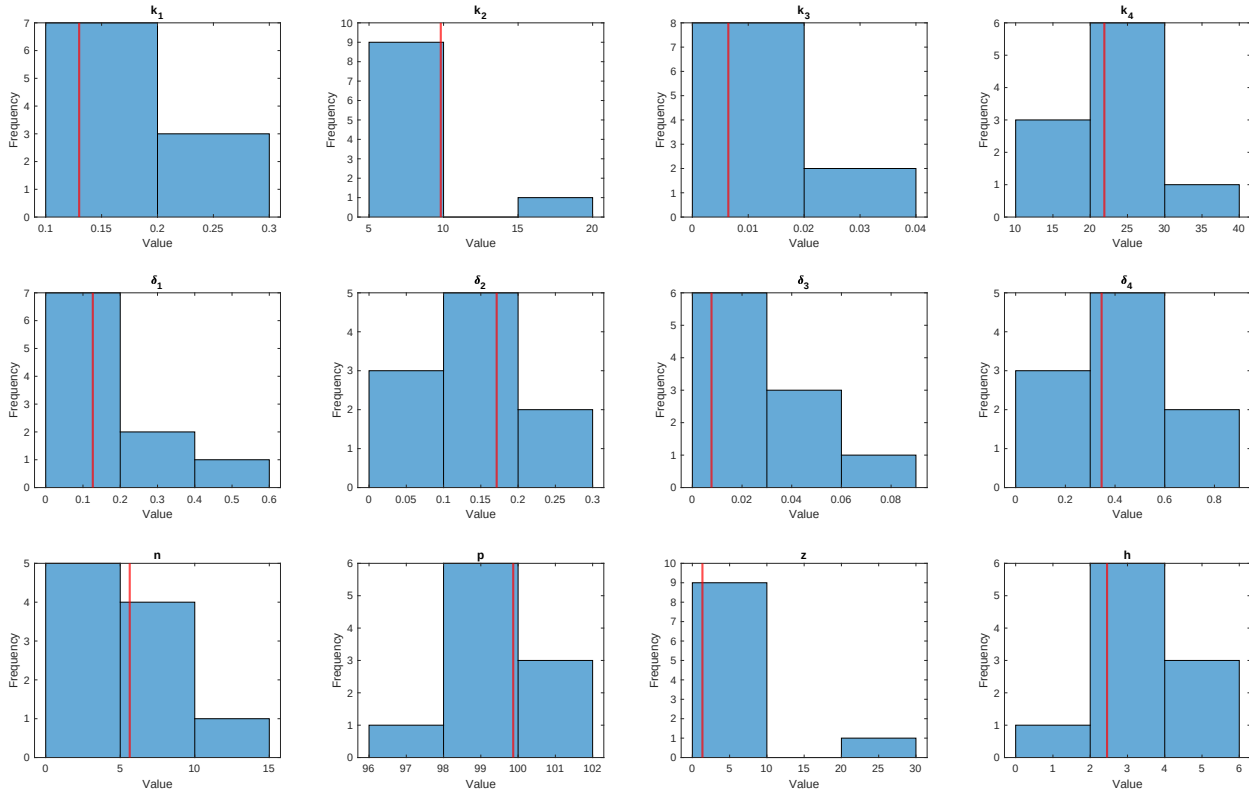

Figure A8. Histogram of best fit parameter distributions when fitting the IGG model to individual pigs. The red line indicates the best fit parameter value when fitting to the median of all ten pigs.